Supporting Information

Redox and Coordination Behavior of the Hexaphosphabenzene Ligand in [(Cp*Mo)$_2$(μ,η^6:η^6-P$_6$)] Towards the "Naked" Cations Cu$^+$, Ag$^+$, and Tl$^+$

Martin Fleischmann, Fabian Dielmann, Laurence J. Gregoriades, Eugenia V. Peresypkina, Alexander V. Virovets, Sebastian Huber, Alexey Y. Timoshkin, Gábor Balázs, and Manfred Scheer*

ange_201506362_sm_miscellaneous_information.pdf

1   General information

All experiments were performed under an atmosphere of dry argon or nitrogen using standard Schlenk and drybox techniques. Commercially available reagents were used as received without further purification. Solvents were freshly distilled under nitrogen from CaH_2 (CH_2Cl_2, CD_2Cl_2, CH_3CN ,CD_3CN), Na (toluene) or Na/K-alloy (*n*-pentane, *n*-hexane). Solution NMR spectra were recorded on a Bruker Avance 400 spectrometer ([1]H: 400.130 MHz, [31]P: 161.976 MHz, [13]C: 100.613 MHz). The chemical shifts δ are presented in parts per million ppm and coupling constants *J* in Hz. The following samples were used for external reference: TMS (^{1}H, ^{13}C), $CFCl_3$ (^{19}F), H_3PO_4 85 % (^{31}P). ^{31}P{^{1}H} MAS NMR spectra were recorded on a Bruker Avance 300 ([31]P: 121.495 MHz) by Dr. Christian Gröger of the Physics department of the University of Regensburg. The chemical shifts of the MAS NMR spectra are also presented in the δ scale using NaH_2PO_4 as an external standard. X-Band EPR spectra were recorded on a MiniScope MS400 device from Magnettech GmbH with a frequency of 9.5 GHz equipped with a rectangular resonator TE102. ESI-MS spectra were measured on a Finnigan Thermoquest TSQ 7000 mass-spectrometer. EI-MS spectra were recorded on a Finnigan MAT 95 mass-spectrometer .IR spectra were recorded on a VARIAN FTS-800 FT-IR spectrometer in CH_2Cl_2 solution or the solid substances were grinded together with dried KBr and pressed to pellets. The starting materials [Cp*Mo(CO)$_2$]$_2$,[1] Ag[TEF],[2] Ag[FAl],[3] [Cu(*o*-DFB)$_2$][TEF][4] (*o*-DFB = *ortho*-difluorobenzene), Tl[TEF][5] were prepared according to the literature procedure.

2   Syntheses of described compounds

2.1   Synthesis of [(Cp*Mo)$_2$(μ,η^6:η^6-P$_6$)] (1) and [(Cp*Mo)$_2$(μ-P$_{10}$)] (2)

The synthesis of **1** was reported in the literature with 1% yield after chromatographic work up.[6] During this investigation we developed a new high yield synthesis that is described below.
[Cp*Mo(CO)$_2$]$_2$ 1.94 g (3.38 mmol, 1eq.) and P$_4$ 1.96 g (15.8 mmol, 3.1eq.) are dissolved in 100 mL of diisopropylbenzene (DIB) and heated to reflux. IR spectroscopy showed the disappearance of any CO stretching bands after 90 minutes. (Complex **1** is thermally stable. Therefore, a reaction time of 24 h reflux gives similar results.) The heating was removed and the reaction was slowly cooled down to room temperature whereby a light brown solid precipitated from the solution. The crude product (1.88 g) was filtered off, washed with *n*-pentane (3 × 30 mL) and dried in vacuum. Recrystallization from warm CH_2Cl_2 affords **1** as medium brown crystals.

Yield	1.88 g (crude), 1.41 g (64%, pure)
^{1}H-NMR (CD_2Cl_2)	δ/ppm = 0.56 (s; C_5Me_5)
^{31}P{^{1}H}-NMR (CD_2Cl_2)	δ/ppm = −314.3 (s)
Elemental analysis	calc. for $C_{20}H_{30}Mo_2P_6$ C: 37.06%, H: 4.67%; found C: 37.00%, H: 4.83%.

After recrystallization of **1** from CH_2Cl_2, we were able to identify very few tiny dark red crystals adhered to large crystals of **1**. Single-crystal X-ray analysis revealed the molecular structure of [(Cp*Mo)$_2$(μ-P$_{10}$)] (**2**). Unfortunately, we were not able to isolate enough of this compound for NMR characterization.

Yield	very few crystals (not determinable ~ below 0.1%)
EI-MS (CH_2Cl_2)	*m/z* (%) = 647.9 (100) [(Cp*Mo)$_2$P$_6$]$^+$, 772.0 (5) [(Cp*Mo)$_2$P$_{10}$]$^+$.

2.2   Synthesis of [(Cp*Mo)$_2$(μ,η^6:η^6-P$_6$)][TEF] (3a)

The *cyclo*-P$_6$ ligand complex **1** is easily oxidized by Ag$^+$ or Cu$^+$ in pure CH_2Cl_2.

Method 1:

A mixture of Ag[Al{OC(CF$_3$)$_3$}$_4$]•CH$_2$Cl$_2$ (135 mg, 0.12 mmol), [(Cp*Mo)$_2$(μ,η^6:η^6-P$_6$)] (**1**) (75 mg, 0.12 mmol) and CH$_2$Cl$_2$ (20 mL) was stirred for 72 h at room temperature in the dark. The dark teal solution was filtered over diatomaceous earth, which was subsequently washed with CH$_2$Cl$_2$ (2 × 2 ml), and the combined filtrate and washings were concentrated to about one fifth of the original volume (~ 5 mL). The concentrated solution was carefully layered with *n*-pentane (5 mL) and stored in a freezer (–28 °C). Compound **3a** can be isolated as dark teal plates.

Yield   160 mg (86%)

Method 2:

[Cu(*o*-DFB)$_2$][TEF] (50 mg; 1 eq., 0.04 mmol) and [(Cp*Mo)$_2$(μ,η^6:η^6-P$_6$)] (**1**) (26 mg, 1eq., 0.04 mmol) were weighed together as solids. The addition of CH$_2$Cl$_2$ (~ 10 mL) lead to an immediate color change from brown to a dark teal solution. After stirring for 3 h the solution was filtered over diatomaceous earth. The dark teal clear solution was carefully layered with *n*-pentane and stored at +4 °C. Compound **3a** was isolated as dark teal plates. The crystals were filtered off, washed with *n*-pentane (3 × 5 mL) and dried in vacuum.

Yield	62 mg (80%)
^{1}H-NMR (CD$_2$Cl$_2$)	δ/ppm = 4.08 (br, $\omega\frac{1}{2}$ = 16 Hz, CH$_3$)
^{13}C{^{1}H}-NMR (CD$_2$Cl$_2$)	δ/ppm = 90.28 (s, Cp*), 4.92 (s, CH$_3$), 121.64 (q, $^1J_{C,F}$ = 294 Hz, CF$_3$)
^{19}F{^{1}H}-NMR (CD$_2$Cl$_2$)	δ/ppm = –75.03 (s, CF$_3$)
^{31}P{^{1}H}-NMR (CD$_2$Cl$_2$)	δ/ppm = no signal detectable between –1200 and +1200 ppm (paramagnetic)
^{27}Al-NMR (CD$_2$Cl$_2$)	δ/ppm = 33.62 (s, [Al(OC(CF$_3$)$_3$)$_4$]$^-$)
X-band EPR (77 K, CD$_2$Cl$_2$)	g_{iso} = 2.019
Evans-method	μ_{eff} = 1.67 μ_B (one unpaired electron)
ESI-MS (CH$_2$Cl$_2$)	cations: *m/z* (%) = 647.9 (100) [(Cp*Mo)$_2$P$_6$]$^+$; anions: *m/z* (%) 966.9 (100) [Al(OC(CF$_3$)$_3$)$_4$]$^-$.
IR (KBr)	$\tilde{v}$/cm^{-1} = 2983 (w), 2924 (w), 1482 (w), 1451 (w), 142 (w), 1383 (m), 1353 (m), 1302 (s), 1277 (s), 1242 (s), 1220 (s), 1170 (m), 1101 (m), 1028 (m), 974 (s), 838 (w), 756 (w), 728 (s), 560 (w), 537 (m), 448 (m).
Elemental analysis	calc. for C$_{36}$H$_{30}$Mo$_2$P$_6$AlO$_4$F$_{36}$ C: 26.77%, H: 1.87%; found C: 26.49%, H: 1.99%.

2.3 Synthesis of [(Cp*Mo)$_2$(μ,η^6:η^6-P$_6$)][FAl] (3b)

Ag[FAl] (79 mg, 1eq., 0.05 mmol) is dissolved in 5 mL of CH$_2$Cl$_2$ to yield a clear colorless solution. [(Cp*Mo)$_2$(μ,η^6:η^6-P$_6$)] (**1**) (33 mg, 1eq., 0.05 mmol) is dissolved in 10 mL of CH$_2$Cl$_2$ to yield a clear medium brown solution. When the Ag$^+$ solution is slowly added to the stirred solution of **1** the color changes to dark green and a black precipitate of Ag^0 is formed. After stirring for 3 h the solution is filtered and subsequently carefully layered with *n*-hexane. After storage at +4 °C for some days compound **3b** can be obtained as dark green blocks. The solution is decanted off. The crystals are washed with *n*-hexane (3 × 10 mL) and dried in vacuum.

Yield	59 mg (58%)
^{1}H-NMR (CD$_2$Cl$_2$)	δ/ppm = 4.21 (br, $\omega\frac{1}{2}$ = 17 Hz, CH$_3$)
^{13}C{^{1}H}-NMR (CD$_2$Cl$_2$)	δ/ppm = 89.82 (s, Cp*), 4.55 (s, CH$_3$)
^{19}F{^{1}H}-NMR (CD$_2$Cl$_2$)	δ/ppm = –112.3 (d, $J_{F,F}$ = 275 Hz, 2F), –117.1 (d, $J_{F,F}$ = 279 Hz, 2F), –121.5 (d, $J_{F,F}$ = 277 Hz, 2F), –127.7 (s, 2F), –130.4 (d, $J_{F,F}$ = 275 Hz, 2F), –136.8 (d, $J_{F,F}$ = 276 Hz, 2F), –140.7 (d, $J_{F,F}$ = 277 Hz, 1F), –153.9 (t, $J_{F,F}$ = 22 Hz, 1F), –164.6 (t, $J_{F,F}$ = 18 Hz, 1F), –172.0 ppm (s, AlF);
^{31}P{^{1}H}-NMR (CD$_2$Cl$_2$)	δ/ppm = no signal detectable between –1200 and +1200 ppm (paramagnetic)
X-band EPR (77 K, solid)	g_{iso} = 2.024

2.4 Synthesis of [Ag{(Cp*Mo)$_2$(μ,η^6:η^6:η^2-P$_6$)}$_2$][TEF] (4b)

Ag[Al{OC(CF$_3$)$_3$}$_4$]•CH$_2$Cl$_2$ (87 mg, 1eq., 0.075 mmol) and [(Cp*Mo)$_2$(μ,η^6:η^6-P$_6$)] (**1**) (110 mg, 2.2eq., 0.165 mmol) were combined as solids. Addition of 15 mL toluene afforded a medium brown suspension. Upon slow addition of a small amount of CH$_2$Cl$_2$ (~ 3 mL) under constant stirring the solution turned bright orange and most of the precipitate dissolved. After 30 minutes the brown precipitate was filtered off ant the clear orange solution was layered with the fivefold amount of toluene and subsequently stored at +4 °C. Compound **4b** can be obtained as light orange crystals forming on the glass walls after a few days. The crystals are freed from the mother liquor, washed with toluene (2 × 50 mL) and dried in vacuum. The crystals show a rather low solubility in CH$_2$Cl$_2$ compared to the analogues Cu$^+$ compound **4a** and decomposes quickly to the oxidized compound **3a** and elemental Ag.

2.5 Synthesis of [Cu{(Cp*Mo)$_2$(μ,η^6:η^6:η^2-P$_6$)}$_2$][TEF] (4a, 5)

The addition of toluene or MeCN to this reaction is necessary to prevent the oxidation of [(Cp*Mo)$_2$(μ,η^6:η^6-P$_6$)] (**1**) by Cu$^+$.

*Isolation of [Cu{(Cp*Mo)$_2$(μ,η^6:η^6:η^2-P$_6$)}$_2$][TEF] as dist. square planar form 4a:*
[Cu(*o*-DFB)$_2$][TEF] (100 mg, 1eq., 0.079 mmol) was dissolved in 10 mL toluene and 2 mL of CH$_2$Cl$_2$ affording a clear colorless solution. [(Cp*Mo)$_2$(μ,η^6:η^6-P$_6$)] (**1**) (104 mg, 2eq., 0.159 mmol) was suspended in 5 mL toluene and 1 mL CH$_2$Cl$_2$. The Cu$^+$ solution was slowly added to the solution of **1** while stirring, resulting in a bright orange solution with very few precipitate. After 30 minutes, the solution was filtered and carefully layered with the twofold amount of *n*-pentane. After 3 days storage at +4 °C, compound **4a** can be isolated as orange needles. These were filtered off, washed with *n*-pentane (3 × 10 mL) and dried in vacuum.

*Isolation of [Cu{(Cp*Mo)$_2$(μ,η^6:η^6:η^2-P$_6$)}$_2$][TEF] as dist. tetrahedral form 5:*
[Cu(*o*-DFB)$_2$][TEF] (63 mg, 1eq., 0.05 mmol) and [(Cp*Mo)$_2$(μ,η^6:η^6-P$_6$)] (**1**) (65 mg, 2eq., 0.1 mmol) were combined as solids. The addition of pristine toluene (~ 80 mL) while stirring resulted in the formation of a bright orange solution while most of the solids were dissolved and only a small amount of dark brown to black residue remained. After 30 minutes the solution was filtered and subsequently

layered with the fivefold amount of *n*-hexane. Storage of this layered system at +4 °C for several days affords orange blocks as the main product next to a few very thin orange needles and some white precipitate. The orange needles and the white precipitate were not suitable for X-ray diffraction analysis. The fine orange needles and the precipitate can easily be removed from the orange crystals by washing them with *n*-hexane (3 × 50 mL) and decanting off the washings while the larger orange crystals settle on the ground. After this washing the crystals are dried in vacuum.

Yield	35 mg (30%)
^{1}H-NMR (CD$_2$Cl$_2$)	δ/ppm = 0.93 (s, CH$_3$)
^{13}C{^{1}H}-NMR (CD$_2$Cl$_2$)	δ/ppm = 97.28 (s, Cp*), 12.05 (s, CH$_3$), 121.65 (q, $^1J_{C,F}$ = 295 Hz, CF$_3$)
^{19}F{^{1}H}-NMR (CD$_2$Cl$_2$)	δ/ppm = −75.75 (s, CF$_3$)
^{31}P{^{1}H}-NMR (CD$_2$Cl$_2$, 300 K)	δ/ppm = −290.4 (br, $\omega_{1/2}$ = 126 Hz, P$_6$)
^{31}P{^{1}H}-NMR (CD$_2$Cl$_2$, 213 K)	δ/ppm = −293.4 (br, $\omega_{1/2}$ = 71 Hz, P$_6$, see section 5.3)
^{31}P{^{1}H}-MAS-NMR (293 K, f = 30 kHz)	δ/ppm = −288.8 (br, $\omega_{1/2}$ = 937 Hz, P$_6$, see section 5.1)
ESI-MS (CH$_2$Cl$_2$)	cations: *m/z* (%) = 647.9 (100) [(Cp*Mo)$_2$P$_6$]$^+$, 751.9 (42) [Cu{(Cp*Mo)$_2$P$_6$}(MeCN)]$^+$, 1360.7 (11) [Cu{(Cp*Mo)$_2$P$_6$}$_2$]$^+$; anions: *m/z* (%) 966.9 (100) [Al(OC(CF$_3$)$_3$)$_4$]$^-$.
IR (KBr)	$\tilde{\nu}$/cm^{-1} = 2970 (w), 2911 (w), 2859 (w), 1481 (w), 1449 (w), 1424 (w), 1379 (m), 1352 (m), 1301 (s), 1277 (s), 1241 (s), 1218 (s), 1164 (m), 1025 (m), 974 (s), 831 (w), 728 (s), 560 (w), 537 (m), 446 (m).
Elemental analysis	calc. for C$_{56}$H$_{60}$CuMo$_4$P$_{12}$AlO$_4$F$_{36}$ C: 28.90%, H: 2.60%; found C: 28.71%, H: 2.59%.

2.6   Synthesis of [Tl{(Cp*Mo)$_2$(μ,η^6:η^6:η^2-P$_6$)}$_2$]$_n$[TEF]$_n$ (6)

[(Cp*Mo)$_2$(μ,η^6:η^6-P$_6$)] (**1**) (50 mg, 2 eq., 0.08 mmol) and Tl[TEF] (45 mg, 1eq., 0.04 mmol) were combined as solids in a flask. Immediately upon the addition of CH$_2$Cl$_2$ (10 mL) a dark red solution formed. After 2 h of stirring at room temperature, the solution was filtered and carefully layered with the fivefold amount of *n*-pentane. After storage at +4 °C for several days compound **6** can be obtained as dark red plates. The crystals are filtered off, washed with *n*-pentane (3 × 5 mL) and dried in vacuum.

Yield	65 mg (68%)
^{1}H-NMR (CD$_2$Cl$_2$)	δ/ppm = 0.83 (s; Cp*)
^{13}C{^{1}H}-NMR (CD$_2$Cl$_2$)	δ/ppm = 12.05 (s; C$_5$(CH$_3$)$_5$), 97.28 (s; C$_5$(CH$_3$)$_5$), 121.65 (q, $^1J_{F,C}$ = 296 Hz; CF$_3$)
^{19}F{^{1}H}-NMR (CD$_2$Cl$_2$)	δ/ppm = −75.7 (s; CF$_3$)
^{31}P{^{1}H}-NMR (CD$_2$Cl$_2$, RT)	no signal can be resolved;
^{31}P{^{1}H}-NMR (CD$_2$Cl$_2$, 193 K)	δ/ppm = −305.5 (br, $\omega_{1/2}$ = 1303 Hz) (see section 5.5)
^{31}P{^{1}H}-MAS-NMR (293 K, 27 kHz)	−291.1 (br, $\omega_{1/2}$ = 1530 Hz)
^{31}P{^{1}H}-MAS-NMR (343 K, 25 kHz)	−289.6 (br, $\omega_{1/2}$ = 300 Hz, small signal), −309.2 (br, $\omega_{1/2}$ = 260 Hz, large signal, see section 5.2)
ESI-MS (CH$_2$Cl$_2$)	cations: *m/z* (%) = 204.38 (100) Tl$^+$, 648.17 (98) [(Cp*Mo)$_2$P$_6$]$^+$, 852.56 (3) [Tl{(Cp*Mo)$_2$P$_6$}]$^+$; anions: 967.0 (100) [Al{OC(CF$_3$)$_3$}$_4$]$^-$.
IR (KBr)	$\tilde{\nu}$/cm^{-1} = 2960 (w), 2917 (w), 2851 (vw), 1636 (m), 1384 (w), 1302 (s), 1277 (s), 1242 (s), 1220 (vs), 1166 (m), 1025 (m), 974 (vs), 728 (s), 669 (m).
Elemental analysis	calc. for TlAlO$_4$Mo$_4$P$_{12}$C$_{56}$F$_{36}$H$_{60}$ C: 27.25%, H: 2.45%; found C: 27.62%, H: 2.30%.

3 Determination of the magnetic moment of 3a by the Evans method

The magnetic moment μ_{eff} of the oxidized *cyclo*-P_6 complex $[\mathbf{1}]^+$ in the compound $[\mathbf{1}][TEF]$ (**3a**) was determined by the Evans NMR method,[7,8,9,10] using equation (1).[11]

$$\mu_{eff} = 798\sqrt{T \cdot \chi_m} \qquad (1)$$

$$\chi_m = \frac{3 \cdot \Delta f}{1000 \cdot f \cdot c}$$

χ_m = molar susceptibility of the sample in $m^3\ mol^{-1}$, Δf = chemical shift difference of the residual solvent signal inside and outside of the capillary in Hz, f = frequency of the NMR spectrometer, c = concentration of the sample in $mol\ dm^{-3}$, T is the measurement temperature in K.

The measurement resulted in a μ_{eff} of 1.67 μ_B for **3a** which is in good agreement with one unpaired electron.

4 Representation of the X-Band EPR spectra of 3a and 3b

The oxidized *cyclo*-P_6 complex cation $[(Cp^*Mo)_2(\mu,\eta^6{:}\eta^6{-}P_6)]^+$ (= $[\mathbf{1}]^+$) is paramagnetic and X-band EPR spectra (f = 9.5 GHz) were recorded for. $[\mathbf{1}][TEF]$ (**3a**) in CD_2Cl_2 solution and for $[\mathbf{1}][FAl]$ (**3b**) in the solid state. For both compounds we were unable to resolve any signal at room temperature, but upon cooling to 77 K we could resolve one broad signal for each sample without any hyperfine coupling at g_{iso} = 2.024 (**3b**) or g_{iso} = 2.019 (**3a**).
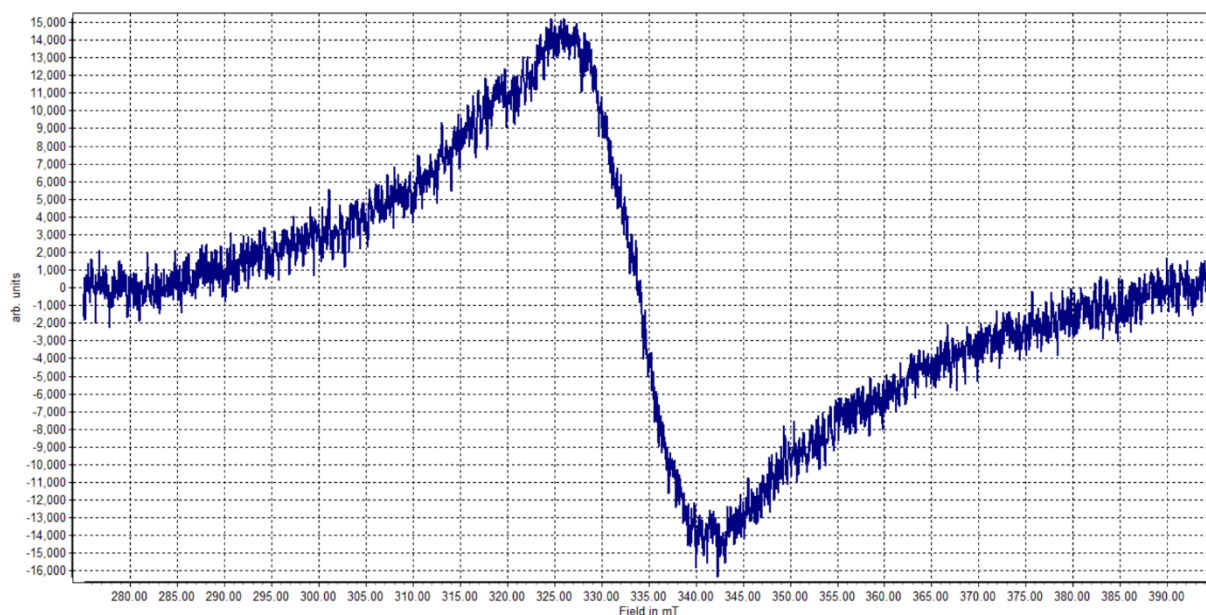
Figure 1. EPR spectrum of compound 3a in CD_2Cl_2 measured at 77 K.
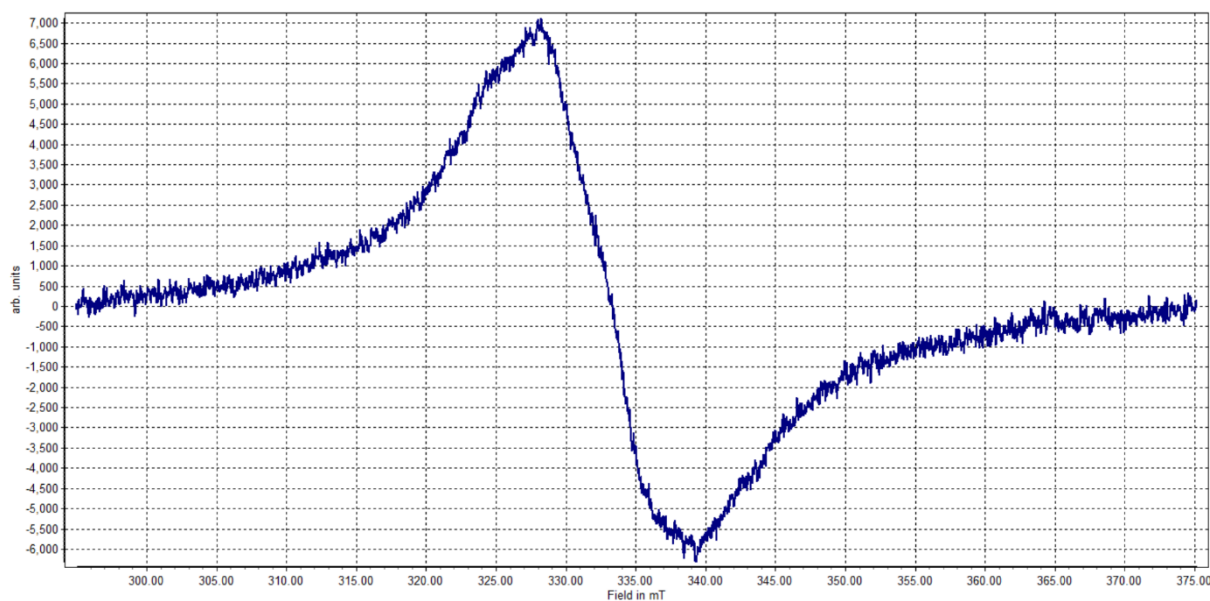
Figure 2. EPR spectrum of compound 3b as crystalline sample cooled to 77 K.

5 Selected VT and MAS-NMR spectra

5.1 MAS-NMR of [Cu{(Cp*Mo)$_2$(μ,η^6:η^6:η^2-P$_6$)}$_2$][TEF] (4a)

293 K, 30 kHz
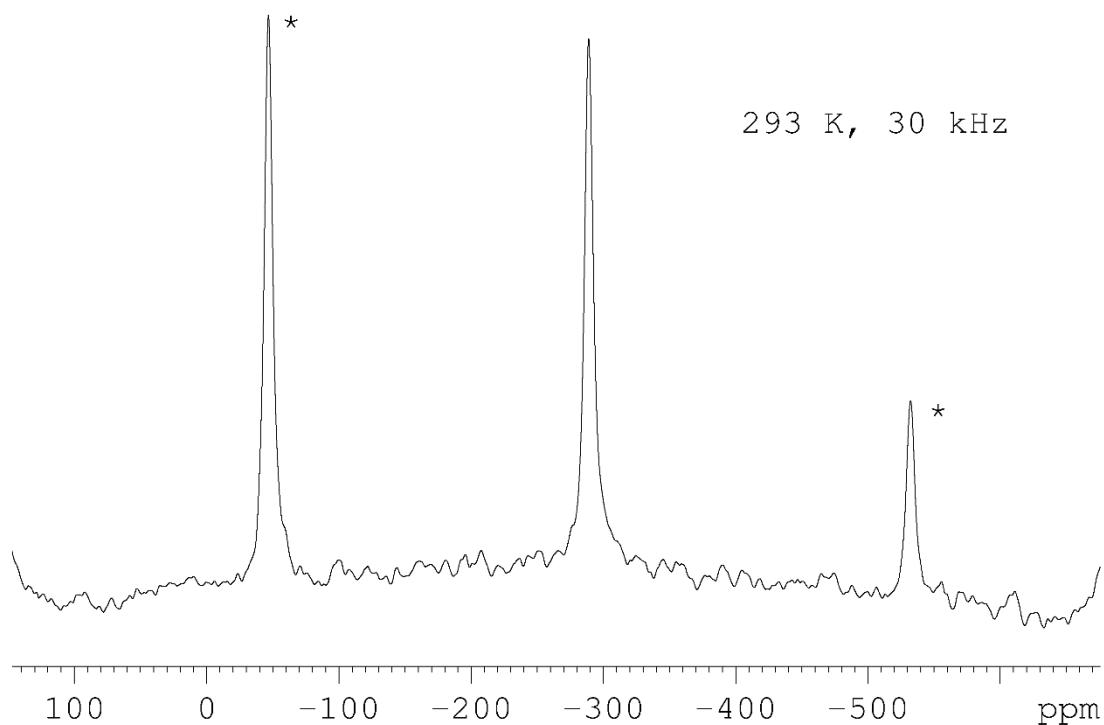
Figure 3. ^{31}P{^{1}H} MAS NMR spectra of the Cu$^+$ compound isolated as its square planar isomer 4a. The absolute signal positions were confirmed by measurement at different rotation frequencies. * rotation side bands.

5.2   MAS-NMR of $[Tl\{(Cp^*Mo)_2(\mu,\eta^6:\eta^6:\eta^2-P_6)\}_2]_n[TEF]_n$ (6)

293 K, 27 kHz

343 K, 25 kHz

-250   -300   -350   ppm
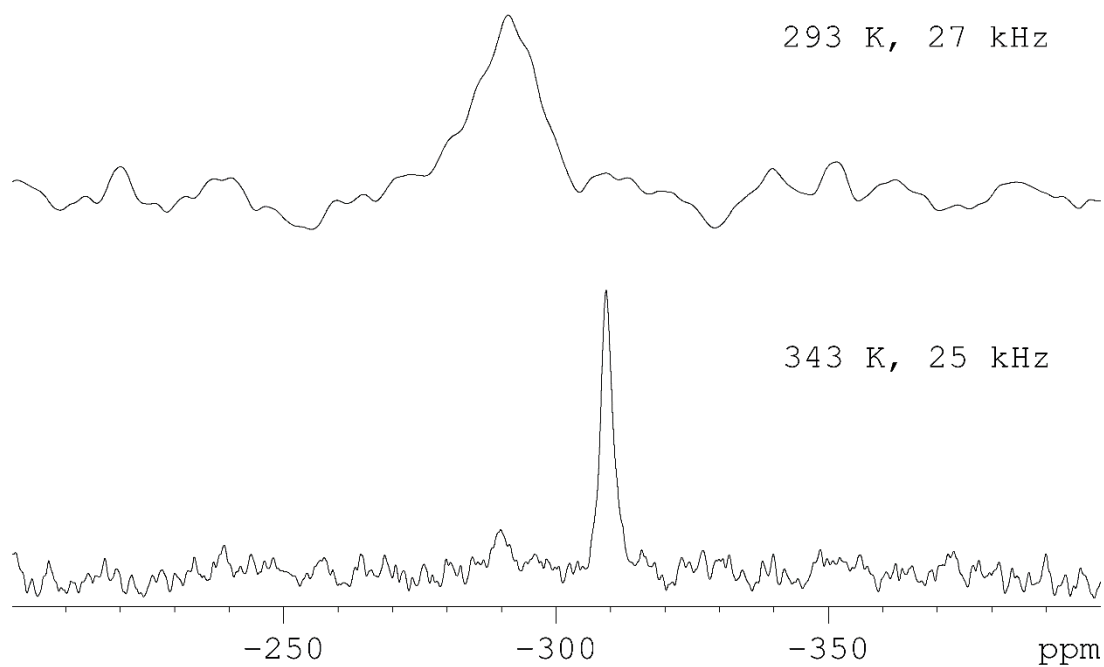
Figure 4. $^{31}P\{^1H\}$ MAS NMR spectra of compound 6. The absolute signal positions were confirmed by measurement at different rotation frequencies.

5.3 VT-NMR of [Cu{(Cp*Mo)$_2$(μ,η^6:η^6:η^2-P$_6$)}$_2$][TEF] (4a, 5)
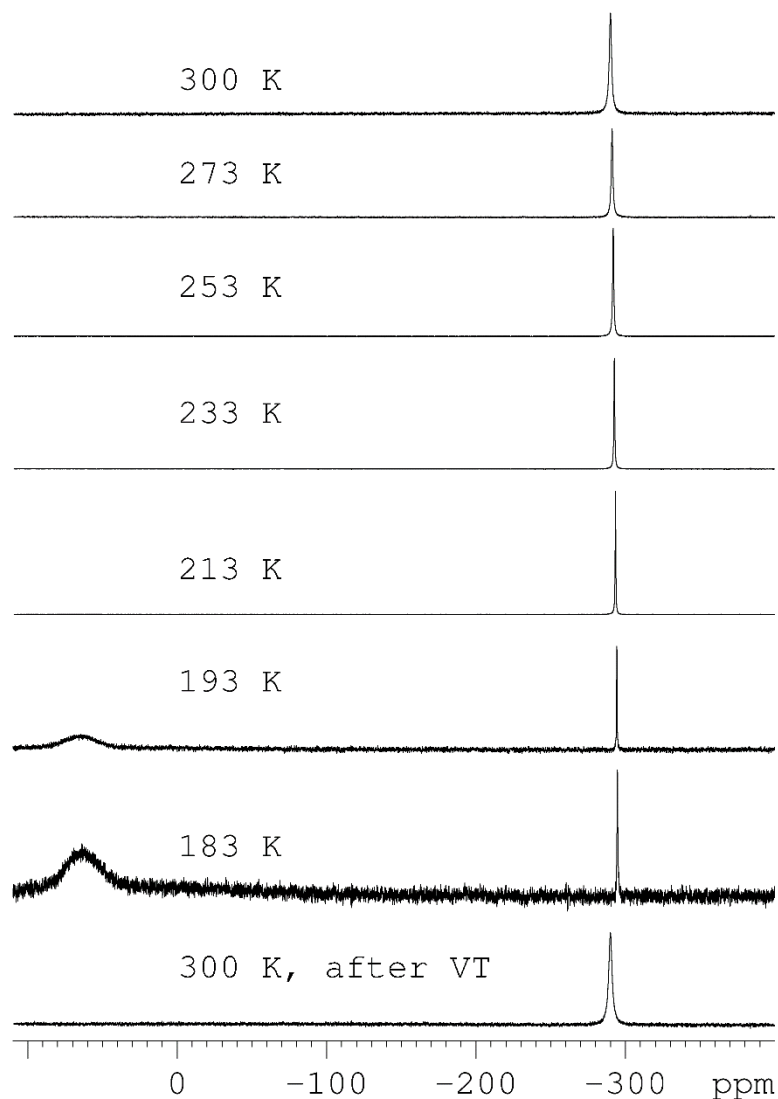
Figure 5. ^{31}P{^{1}H} VT-NMR experiment of [Cu(1)$_2$][TEF] in CD$_2$Cl$_2$ cooling from 300 K to 183 K and warming up again to 300 K.

The Cu compounds **4a** and **5** show a broad singlet at –290.4 ppm in the ^{31}P{^{1}H} NMR spectrum at room temperature revealing the chemical and magnetic equivalence of all P atoms of the *cyclo*-P$_6$ ligands on the NMR timescale. This is most probably caused by fast underlying equilibria including fast rotation of the P$_6$ rings. Upon cooling the singlet remains almost unchanged showing the highly dynamic coordination behavior persists even at low temperatures.

When the solution is cooled below 193 K a new very broad signal arises next to the singlet at +66 ppm which may arise from precipitation of the product. After warming the sample up again, the new signal vanishes and only the singlet of the pure compound **4a** or **5** can be observed.

5.4 VT-NMR of [Ag{(Cp*Mo)$_2$(μ,η^6:η^6:η^2-P$_6$)}$_2$][TEF] (4b)
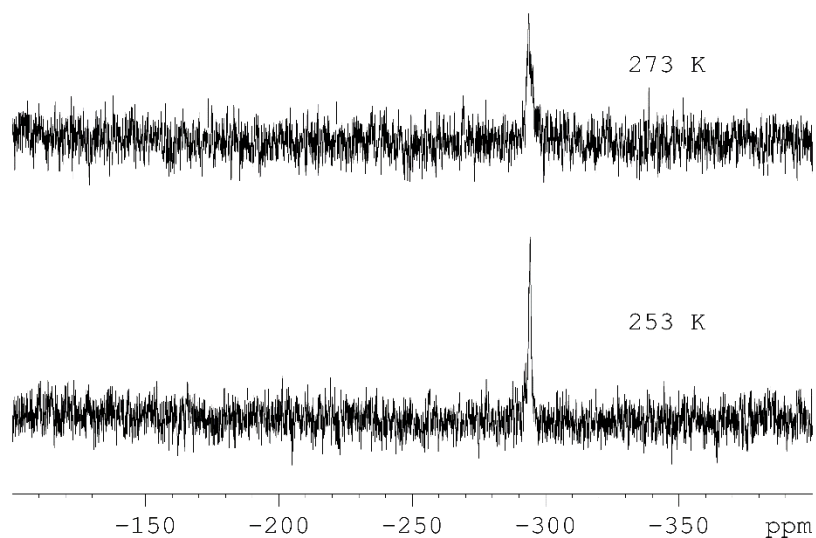
Figure 6. ^{31}P{^{1}H} VT NMR spectrum of 4b recorded upon warming a crystalline sample of 4b in CD$_2$Cl$_2$. The spectra for temperatures below 253 K or above 273 K did not show any signal because of the limited solubility and the fast decomposition.

5.5 VT-NMR of [Tl{(Cp*Mo)$_2$(μ,η^6:η^6:η^2-P$_6$)}$_2$]$_n$[TEF]$_n$ (6)
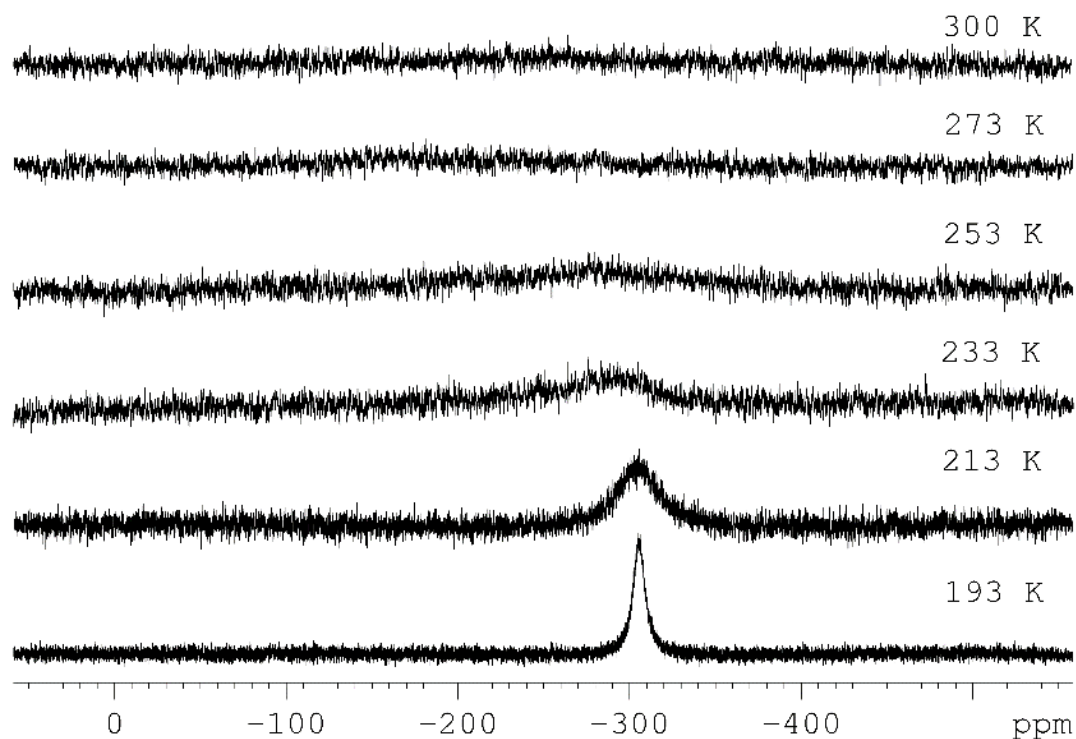
Figure 7. ^{31}P{^{1}H} VT-NMR spectrum of compound 6 in CD$_2$Cl$_2$.

At room temperature no signal can be resolved in the ^{31}P{^{1}H} NMR spectrum of compound **6** in CD$_2$Cl$_2$. Upon cooling below 213 K a very broad signal can be observed at –305.5 ppm.

6 X-ray structure determination

6.1 General considerations

All crystal manipulations were performed under mineral oil or perfluorinated oil. The diffraction experiments were performed at 123 K on an Agilent Technologies Gemini R Ultra diffractometer or an Agilent SuperNova diffractometer with Cu-K_α or Mo-K_α radiation. Crystallographic data together with the details of the experiments are given in Table 1 and Table 2. The cell determination, data reduction and absorption correction for all compounds were performed with the help of the CrysAlis PRO software by Agilent Technologies Ltd. The full-matrix least-square refinement against F^2 was done with ShelXL. During the refinement several restraints and constraints had to be applied. For the description of the refinement strategy we list the commonly used syntax for the ShelXL program (DFIX, SADI, SIMU, ISOR, EADP). All atoms except hydrogen were refined anisotropically if not described otherwise. The H atoms were calculated geometrically and a riding model was used during refinement process. Graphical material was created with the free software Olex2. CCDC-1411077 (**1**), CCDC-1411078 (**2**), CCDC-1411079 (**3b**), CCDC-1411080 (**4a**), CCDC-1411081 (**4b**), CCDC-1411082 (**5**), and CCDC-1411083 (**6**) contain the supplementary crystallographic data for this paper. These data can be obtained free of charge from The Cambridge Crystallographic Data Centre via www.ccdc.cam.ac.uk/data_request/cif.

6.2 Special comments on the weakly coordinating anion [TEF]

Due to its weakly coordinating nature, the anion [TEF] tends to be disordered in a lot of its solid state structures. The CF_3- as well as whole $(CF_3)_3CO$-groups frequently exhibit rotational disorder by rotation of C–O or C–C bonds, respectively. In some cases even a positional disorder of the whole anion can be observed. To resolve these kinds of disorder which are still present at 100 K good data sets with high resolution are needed. In addition, most of the compounds containing the anion [TEF] show a rather weak diffraction at high angles which proves the X-ray crystallography of these compounds to be a very challenging task. During the refinement of these solid state structures it is common that a series of least-square restraints has to be applied to prevent the results to display an unrealistic geometry or displacement parameters. In rare cases, even good data sets do not enable the refinement of all disorders which usually results in large displacement parameters, especially of the fluorine atoms.

6.3 Crystallographic tables

Table 1. Crystallographic details for the compounds 1, 2, 3b and 4b.

	1	2	3b	4b
formula	$C_{20}H_{30}Mo_2P_6$	$C_{19}H_{28.5}Mo_2P_{9.8}$	$C_{56}H_{30}AlF_{46}Mo_2O_3P_6$	$C_{57}H_{62}AgAlCl_2F_{36}Mo_4O_4P_{12}$
weight [g·mol^{-1}]	648.14	752.30	2029.48	2456.21
Temperature [K]	123.00(14)	123.00(10)	123.1(4)	123.01(10)
crystal system	triclinic	monoclinic	monoclinic	monoclinic
space group	P-1	$P2_1/n$	$C2/c$	$C2/c$
a [Å]	8.25280(10)	8.0528(4)	30.6081(3)	36.3787(4)
b [Å]	8.65580(10)	15.3282(6)	21.83616(15)	16.16213(17)
c [Å]	10.12920(10)	11.4000(6)	21.7617(3)	14.51853(16)
α [°]	101.1590(10)	90	90	90
β [°]	106.0070(10)	104.970(5)	110.4429(13)	101.5137(10)
γ [°]	113.5080(10)	90	90	90
Volume [Å^3]	598.789(13)	1359.41(12)	13628.7(3)	8364.49(16)
Z	1	2	8	4
ρ_{calc} [g·cm^{-3}]	1.797	1.838	1.978	1.950
μ [mm^{-1}]	1.454	13.087	6.080	10.624
absorption correction	gaussian	gaussian	gaussian	gaussian
T_{min}/T_{max}	0.820 / 0.855	0.301 / 0.707	0.434 / 0.727	0.435 / 0.617
$F(000)$	324.0	747.0	7928.0	4808.0
crystal size [mm^3]	0.185 × 0.180 × 0.141	0.202 × 0.082 × 0.030	0.212 × 0.120 × 0.058	0.110 × 0.076 × 0.062
radiation [Å]	MoK_α (λ = 0.71073)	CuK_α (λ = 1.54184)	CuK_α (λ = 1.54184)	CuK_α (λ = 1.54184)
diffractometer	Gemini R Ultra	SuperNova	Gemini R Ultra	SuperNova,
2Θ range [°]	5.852 to 60.088	9.89 to 152.33	5.944 to 133.2	8.28 to 147.416
reflns collected/unique	54934 / 3339	4563 / 2718	56018 / 11876	23765 / 8226
R_{int}/R_{sigma}	0.0324 / 0.0182	0.0320 / 0.0350	0.0461 / 0.0326	0.0286 / 0.0212
data/restraints/parameters	3339 / 0 / 132	2718 / 15 / 166	11876 / 36 / 1092	8226 / 109 / 738
GOF on F^2	1.106	1.069	0.946	1.067
R_1/wR_2 [$I \geq 2\sigma(I)$]	0.0191 / 0.0491	0.0474 / 0.1279	0.0299 / 0.0728	0.0413 / 0.1149
R_1/wR_2 [all data]	0.0210 / 0.0495	0.0549 / 0.1324	0.0357 / 0.0747	0.0440 / 0.1167
max/min $\Delta\rho$ [e·Å^{-3}]	1.40 / –0.48	1.20 / –0.89	0.61 / –0.67	1.24 / –0.85

Table 2. Crystallographic details for the compounds 4a, 5 and 6.

	4a	5	6
formula	$C_{57}H_{62}AlCl_2CuF_{36}Mo_4O_4P_{12}$	$C_{147}H_{160}Al_2Cu_2F_{72}Mo_8O_8P_{24}$	$C_{56.45}H_{60.9}AlCl_{0.9}F_{36}Mo_4O_4P_{12}Tl$
weight [g·mol^{-1}]	2411.88	5114.58	2506.00
Temperature [K]	122.99(13)	123(1)	123.15
crystal system	monoclinic	triclinic	monoclinic
space group	$C2/c$	P-1	$C2/c$
a [Å]	36.4679(6)	16.7510(5)	36.1206(14)
b [Å]	16.1466(3)	17.2703(7)	16.4296(5)
c [Å]	14.4134(2)	18.8355(6)	14.5113(7)
α [°]	90	109.136(3)	90
β [°]	101.863(2)	97.750(3)	100.380(4)
γ [°]	90	108.799(3)	90
Volume [Å^3]	8305.8(2)	4693.8(3)	8470.8(6)
Z	4	1	4
ρ_{calc} [g·cm^{-3}]	1.929	1.809	1.965
μ [mm^{-1}]	9.123	7.604	11.921
absorption correction	analytical	multi-scan	gaussian
T_{min}/T_{max}	0.187 / 0.509	0.75936 / 1.000	0.270 / 0.870
$F(000)$	4736.0	2534.0	4851.6
crystal size [mm^3]	0.332 × 0.216 × 0.101	0.147 × 0.102 × 0.075	0.164 × 0.121 × 0.011
radiation [Å]	CuK_α (λ = 1.5418)	CuK_α (λ = 1.54178)	CuK_α (λ = 1.54184)
diffractometer	SuperNova	SuperNova	SuperNova
2Θ range [°]	6.008 to 136.476	5.886 to 150.866	8.244 to 146.086
reflns collected/unique	68860 / 7599	34771 / 18870	14650 / 8068
R_{int}/R_{sigma}	0.0478 / 0.0166	0.0362 / 0.0472	0.0383 / 0.0464
data/restraints/parameters	7599 / 123 / 758	18870 / 241 / 1261	8068 / 162 / 730
GOF on F^2	1.112	1.053	1.083
R_1/wR_2 [$I \geq 2\sigma(I)$]	0.0472 / 0.1088	0.0665 / 0.1781	0.0836 / 0.2195
R_1/wR_2 [all data]	0.0474 / 0.1090	0.0736 / 0.1867	0.0973 / 0.2272
max/min $\Delta\rho$ [e·Å^{-3}]	1.39 / −1.22	1.82 / −1.11	1.24 / −2.05

6.4 X-ray structure refinement of [(Cp*Mo)$_2$(μ,η^6:η^6-P$_6$)] (1)

The solid state structure of **1** was reported earlier in the literature.[6] The measurement was performed at room temperature (R_1 = 4.1%), therefore we performed another X-ray experiment at low temperature. The solid state structure is depicted in Figure 8.
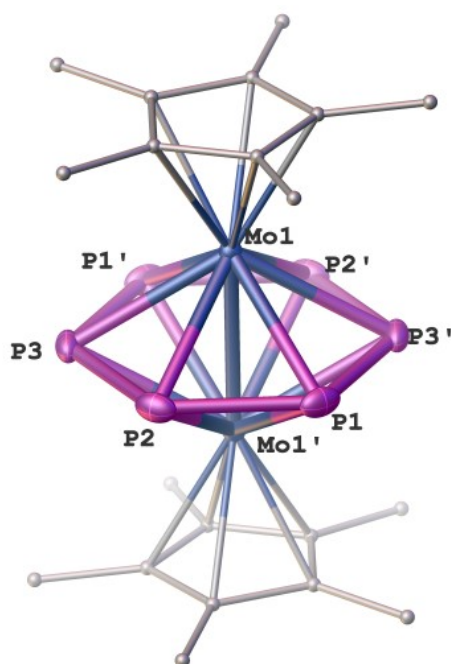
Figure 8. Molecular structure of 1. P purple, Mo blue, C grey; H atoms are omitted and C atoms are depicted as small balls for clarity. Selected bond lengths [Å]: Mo1-Mo1' 2.6463(3), P1-P3' 2.1822(8), P1-P2 2.1833(8), P2-P3 2.1840(8).

Crystals of compounds **1** suitable for X-ray diffraction analysis can be obtained by layering a CH_2Cl_2 solution with pure MeCN. The *cyclo*-P_6 complex crystallizes in the triclinic space group *P*-1 with the molecule occupying the center of symmetry. The refinement was performed without difficulties.

6.5   X-ray structure refinement of [(Cp*Mo)$_2$(μ-P$_{10}$)] (2)

Compound **2** crystallizes in the monoclinic space group *P*2$_1$/*n* with the molecule occupying the center of inversion. Figure 9 shows the *cyclo*-P_{10} ligand of compound **2**. When the structural model containing only the complex with a *cyclo*-P_{10} ligand was refined we observed a residual density peak of ~4 electrons situated at about 0.8 Å next to Mo1. The position and environment of this peak as well as the electron count is in contradiction with the whole molecular complex. Therefore we interpreted it as the second minor position of Mo atom (Mo2). Its occupancy was refined to 5%. Subsequently, we found three additional electron density peaks at reasonable distances to each other and to Mo2 and assigned them as P6, P7 and P8. The Mo and P atoms of the minor part were refined in isotropic approximation. We were unable to localize the minor position of the Cp* ligand due to its negligible contribution to the electron density. Thus, the final model corresponds to a substitutional solid solution of two complexes, a *cyclo*-P_{10} complex **2** and a *cyclo*-P_6 complex **1** mixed in a 95:5 ratio. The model of the disorder is depicted in Figure 10.
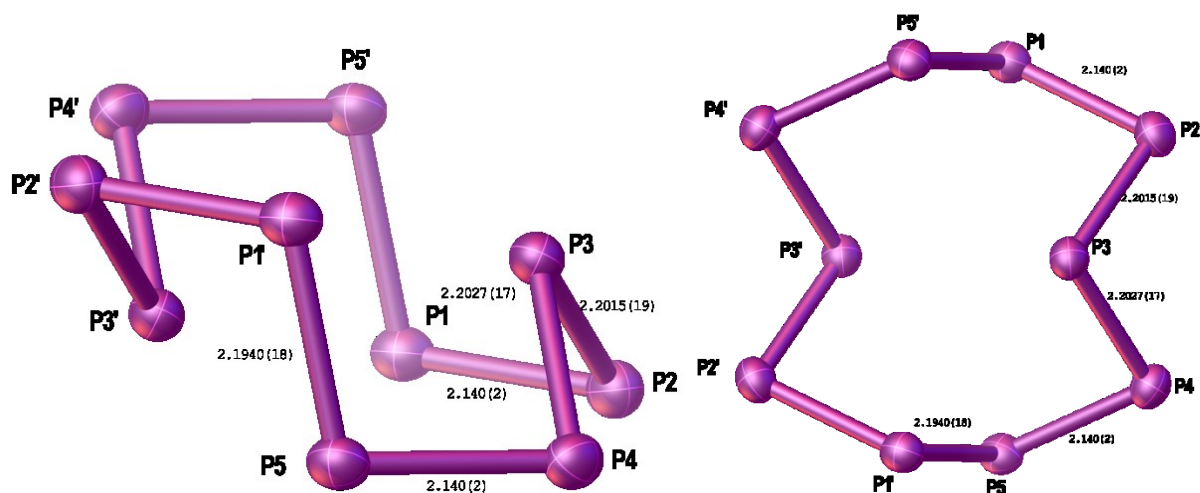
Figure 9. A greatly folded *cyclic* P$_{10}$ ligand of compound 2. Cp*Mo fragments were omitted for clarity. (left) side view (right) front view. Selected atomic distances [Å]: P1-P5' 2.1930(18), P1-P2 2.140(2), P2-P3 2.2015(19), P3-P4 2.2027(17), P4-P5 2.140(2), P2-P4 3.1279(19), P3-P2' 3.174(2), P3-P5' 3.1605(17). Mo1-Mo1' 3.7018(8); Interplanar angle P2-P3-P4-plane to P1-P2-P4-P5-plane 68.18(7)°, interplanar angle P1-P2-P4-P5-plane to P1-P5-P1'-P5'-plane 103.94(7)°.
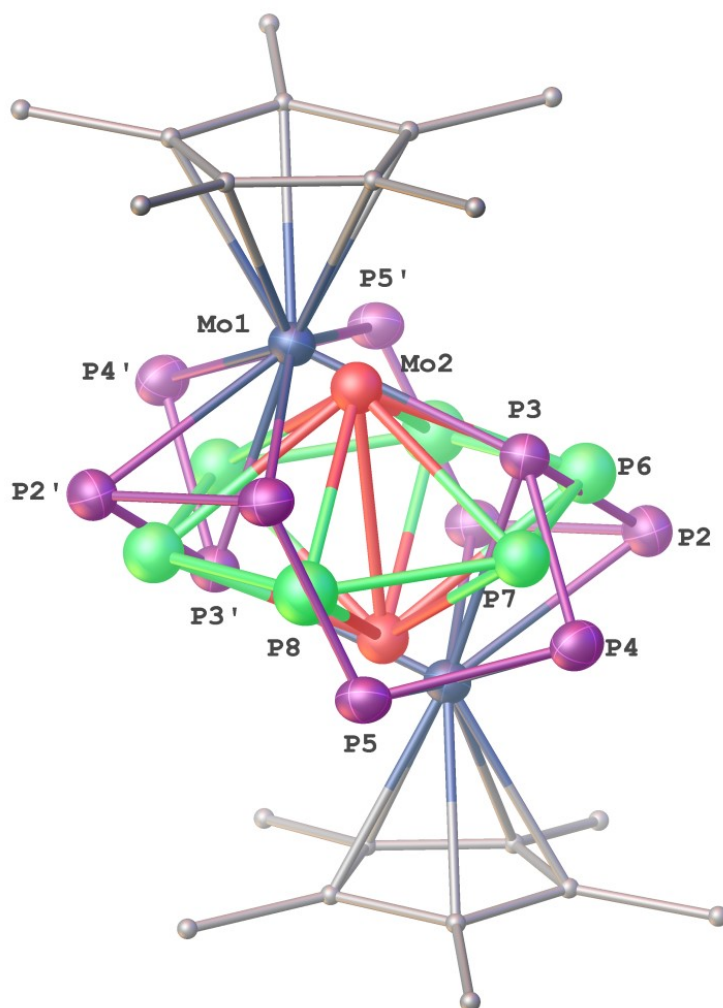
Figure 10. The disordering *cyclo*-P$_{10}$ and *cyclo*-P$_6$ complexes in the crystal structure of compound 2. H atoms are omitted and C atoms are depicted as small balls for clarity. The *cyclo*-P$_{10}$ complex (P purple, Mo blue, C grey) with its Cp* ligands is occupied for 95%, the *cyclo*-P$_6$ complex (P green, Mo red) is occupied for 5% without Cp* ligands. Selected bond lengths [Å]: Mo2-Mo2' 2.613(18), average P-P bond lengths of cyclo-P6 ~2.16 (geometry was restrained by SADI instructions in SHELX!).

6.6 X-ray structure refinement of [(Cp*Mo)$_2$(μ,η^6:η^6-P$_6$)][FAl] (3b)

Crystals of compound **3b** suitable for X-ray diffraction analysis can be obtained by layering a CH$_2$Cl$_2$ solution with *n*-hexane and storage at +4 °C for several days. Compound **3b** crystallizes in the monoclinic space group *C*2/*c*. There are two complex cations occupying the position of a twofold rotation axis (see Figure 11) and one [FAl] anion occupying a general position. One of the P$_6$ rings shows a re-orientational disorder over three close positions (Figure 11 middle, right) while the other one is ordered (Figure 11 left). All P$_6$ rings show a bisallylic distortion with two opposing P-P bonds being significantly elongated (P1-P1', P3-P3', P5-P6, P9-P10, P12-P13). All atoms except hydrogen were refined anisotropically. The displacement parameters of the P atoms with 20% occupancy (P8-P13) had to be restrained with ISOR instruction in SHELX.

Figure 11. The complex cations in the crystal structure of compound 3b. P purple, Mo blue, C grey; H atoms are omitted and C atoms are depicted as small balls for clarity. (left) Structure of the ordered complex cation. (middle) Structure of the second complex cation exhibiting a re-orientational disorder of the P$_6$ ring over three positions. (right) The model of the disorder for the P$_6$ ring. The P$_6$ ring is disordered over three positions in a ratio of 60:20:20. The major orientation (P4 - P7, pink) lie on the twofold axis. The two minor parts are symmetrically equivalent (P8 - P13, red and blue). Selected bond lengths [Å]: Mo1-Mo1' 2.6617(4), P1-P1' 2.2932(13), P1-P2 2.1348(10), P2-P3 2.1384(11), P3-P3' 2.2477(16), Mo2-Mo2' 2.671(2), P4-P5 2.157(3), P5-P6 2.220(3), P6-P7 2.176(3), P8-P9 2.105(9), P9-P10 2.215(8), P10-P11 2.163(7), P11-P12 2.181(8), P12-P13 2.235(8).

6.7 X-ray structure refinement of [Ag{(Cp*Mo)$_2$(μ,η^6:η^6:η^2-P$_6$)}$_2$][TEF] (4b) and [Cu{(Cp*Mo)$_2$(μ,η^6:η^6:η^2-P$_6$)}$_2$][TEF] in its square planar form 4a

The X-ray analysis of the compounds **4a** and **4b** will be discussed together since they are isostructural. Suitable crystals of both compounds can be obtained by layering a concentrated solution in CH$_2$Cl$_2$/toluene with *n*-hexane and storage at +4 °C for several days.

The compounds crystallize in the monoclinic space group *C*2/*c*. The cationic complex [M(P$_6$)$_2$]$^+$ (M =Ag, Cu; P$_6$ = **1**) is occupying the center of inversion. The anion and one CH$_2$Cl$_2$ solvent molecule are situated each on a twofold rotation axis. Both independent fluorinated tert-butoxy groups of the aluminate anion are disordered over two positions (with probability 52:48, 51:49 (Ag); 53:47, 52:48 (Cu)). At the initial stages of the structure refinement most bond distances of the anion were restrained by several DFIX instructions, which were gradually replaced by SADI restraints, which number was maximally reduced, but a lot of them had to be kept even in the final model in order to keep reasonable geometry of the WCA [TEF]. The final model of the anions are shown in Figure 12 and Figure 13 on the right hand side. The displacement parameters of some of the disordered C and F atoms had to be restrained by ISOR, SIMU or DELU or constrained by EADP instructions as well. Some disordered atoms (1 for M = Cu, 7 for M = Ag) were refined in isotropic approximation. The CH$_2$Cl$_2$ solvent molecule is disordered over three positions for M = Ag (43:29:28) and two positions for M = Cu (70:30) The C-Cl distances were restrained in both cases by DFIX instructions. The methylene carbon atoms were refined isotropically and the displacement parameters were equated for M = Ag. The Cl-Cl distances for M = Cu were restrained by DFIX instructions and the displacement parameters of the less occupied Cl atoms were equated. The cationic complexes [M(**1**)$_2$]$^+$ were refined unconstrained (Figure 12 (Ag), Figure 13 (Cu), left hand side).
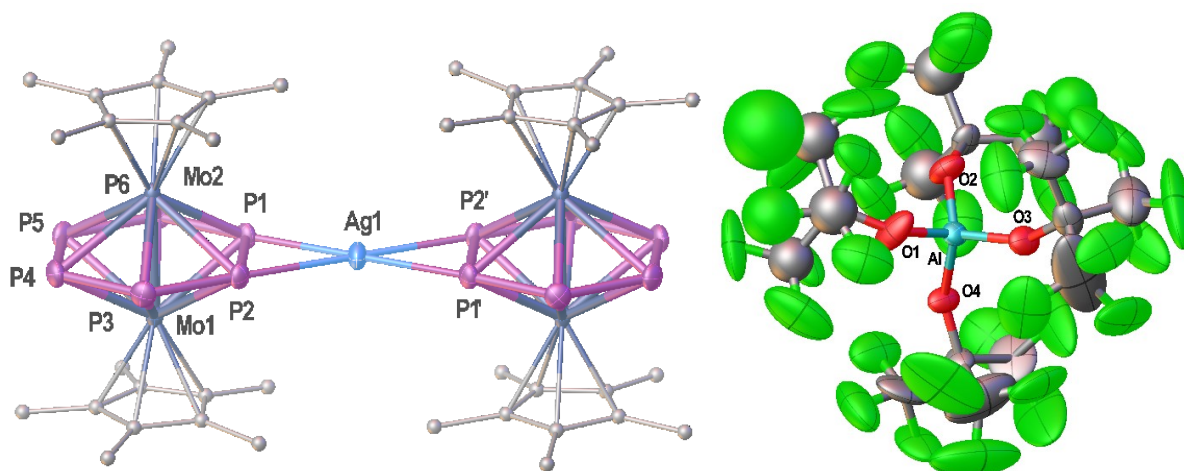
Figure 12. (left) The complex cation from the crystal structure of compound 4b. P purple, Ag light blue, Mo blue, C grey; H atoms are omitted and C atoms are depicted as small balls for clarity. Selected bond lengths [Å]: Ag1-P1 2.5793(10), Ag1-P2 2.6196(10), P1-P2 2.2915(14), P2-P3 2.1653(14), P3-P4 2.1726(15), P4-P5 2.1630(15), P5-P6 2.1671(15), P6-P1 2.1667(14); (right) The final model of the [TEF] anion from the crystal structure of compound 4b.
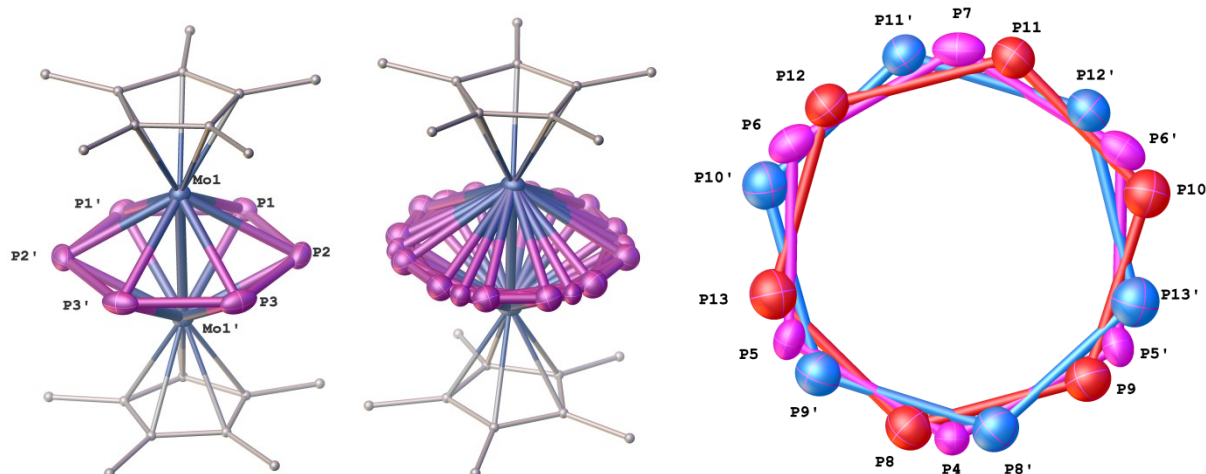

Figure 13. (left) The complex cation in the crystal structure of compound 4a. P purple, Cu orange, Mo blue, C grey; H atoms are omitted and C atoms are depicted as small balls for clarity. Selected bond lengths [Å]: Cu1-P1 2.4354(12), Cu1-P2 2.3927(12), P1-P2 2.2694(16), P2-P3 2.1765(17), P3-P4 2.1685(18), P4-P5 2.1729(18), P5-P6 2.1677(17), P1-P6 2.1808(17); (right) The final model of the [TEF] anion from the crystal structure of compound 4a.

6.8 X-ray structure refinement of [Cu{(Cp*Mo)₂(μ,η^6:η^6:η^2-P₆)}₂][TEF] in its tetrahedral form 5

Suitable crystals of compound **5** for X-ray crystallography can be obtained by layering a toluene solution of **5** with *n*-hexane and storage at +4 °C for several days.

Compound **5** crystallizes in the triclinic space group *P*-1 with two *cyclo*-P₆ ligands **1** coordinated to one Cu atom in a distorted tetrahedral geometry occupying a general position. The [TEF] anion and two toluene solvent molecules are also situated on general positions. Additionally there is another toluene molecule which occupies the center of inversion. The cationic complex [Cu(P₆)₂]⁺ is shown in Figure 14 on the left. In the WCA [TEF] two tert-butoxy groups (containing O1 and O2) showed slight tendency for disorder that was not possible to resolve. The remaining two tert-butoxy groups show a disorder over two positions each related by a rotation around an O-C bond (depicted in Figure 14 right hand side). The occupancies of the two disordered groups were refined to 61:39 and 57:43. The C and F atoms with occupacies below 50% were refined isotropically. The bond distances of the disordered tert-butoxy groups were restrained by several DFIX commands. These DFIX restrains could only partly be replaced by SADI restraints during the final refinement. The displacement parameters of some of these atoms had to be also restrained by ISOR, SIMU and DELU restraints.

The geometry of the two toluene solvent molecules on general positions was restrained to be symmetric by SAME commands with the same ring atoms in opposite order as a reference. The third

toluene solvent molecule is 50% occupied being disordered over an inversion center. The C atoms were refined isotropically and their displacement parameters were equated by EADP instructions.

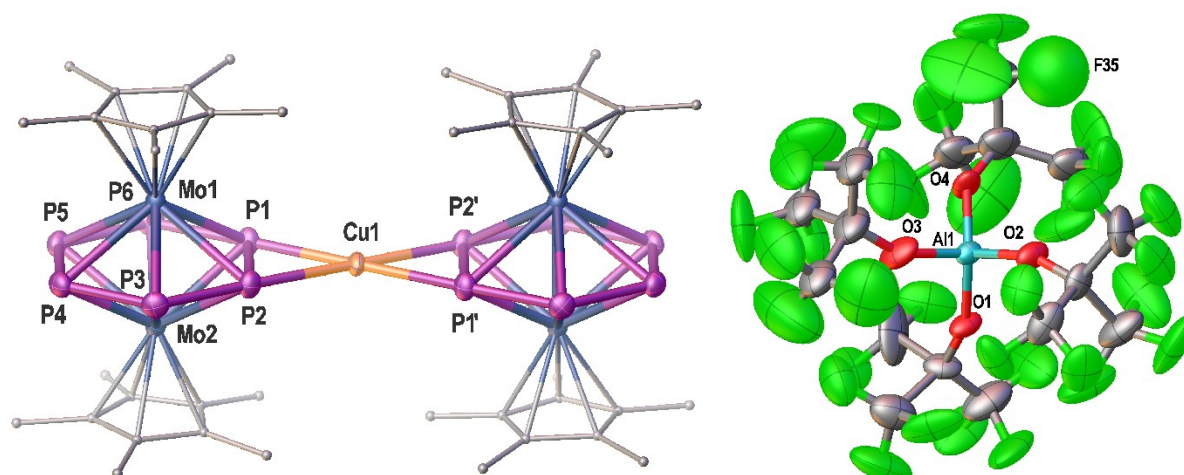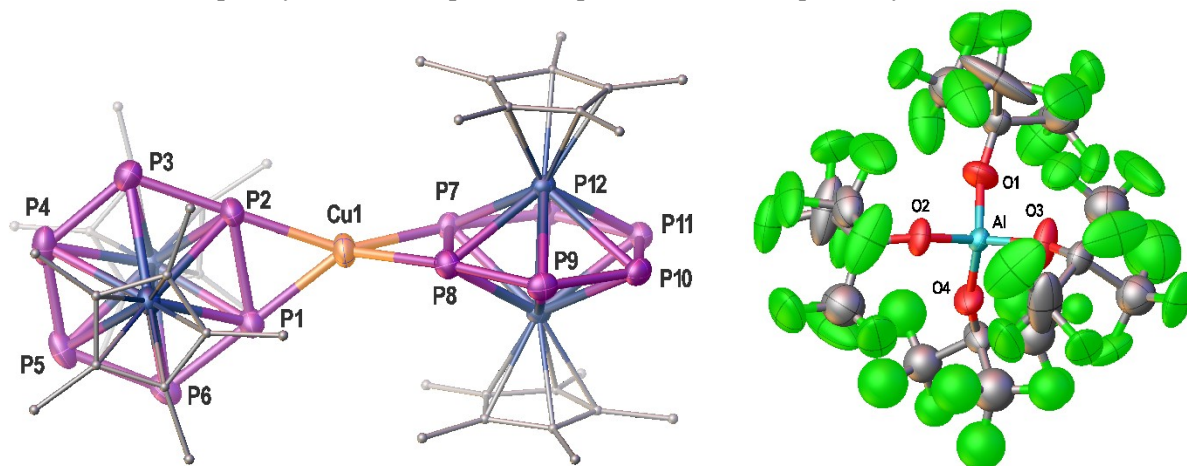**Figure 14. (left) The distorted tetrahedral complex cation in the crystal structure of compound 5. P purple, Cu orange, Mo blue, C grey; H atoms are omitted and C atoms are depicted as small balls for clarity. Selected bond lengths [Å]: Cu1-P1 2.3546(16), Cu1-P2 2.3343(16), Cu1-P7 2.3483(16), Cu1-P8 2.3383(16), P1-P2 2.286(2), P2-P3 2.165(2), P3-P4 2.176(2), P4-P5 2.151(3), P5-P6 2.168(2), P6-P1 2.163(2), P7-P8 2.2876(19), P8-P9 2.1664(19), P9-P10 2.171(2), P10-P11 2.157(2), P11-P12 2.168(2), P12-P7 2.1666(19); Interplanar angle between P1-P2-Cu1 and P7-P8-Cu1 planes 93.5°; (right) The [TEF] anion in the crystal structure of compound 5. For the tert-butoxy groups at O3 and O4 only one orientation is depicted here.**

6.9   X-ray structure analysis of [Tl{(Cp*Mo)$_2$(μ,η^6:η^6:η^2-P$_6$)}$_2$]$_n$[TEF]$_n$ (6)

Details of the X-ray structure refinement

Compound **6** crystallizes in the monoclinic space group *C*2/*c* with a very similar unit cell like the Cu$^+$ and Ag$^+$ compounds **4a** and **4b** (**6** can be regarded as isostructural). The direct coordination environment of Tl$^+$ can be described as a cationic complex [Tl(P$_6$)$_2$]$^+$ (cf. Ag$^+$ and Cu$^+$) which is occupying the center of inversion. The anion and 90% of a CH$_2$Cl$_2$ solvent molecule are situated each on a twofold rotation axis. The structure is severely disordered. The Tl$^+$ cation is disordered around the inversion center. The *cyclo*-P$_6$ ring is disordered over two positions in a 1:1 ratio. The ratio is also in agreement with the distances to the Tl$^+$ cation for both its alternative positions (see Figure 16). One of the Cp* ligands is also disordered by rotation in a 75:25 ratio. The C-C distances of the minor Cp ring position were fixed during the refinement. The hydrogen atoms of the disordered Cp* ligands were refined in geometrically calculated positions for an ordered and in one case for a disordered methyl group. The [TEF] anion is disordered over two positions (1:1 ratio, disorder was refined similar to compound **4a**, see Figure 13 right hand side and exhibits a high thermal motion. During the refinement the geometry of this highly disordered anion had to be restrained by several DFIX, DANG and SADI commands. The number of these restraints was maximally reduced at the end of the refinement. Additionally some displacement parameters of these groups had to be restrained or constrained.

Analysis of the crystal structure

The X-ray structure of **6** is closely related to the crystal structures of the distorted square planar Cu$^+$ and Ag$^+$ compounds **4a** and **4b**. The coordination environment around Tl$^+$ is depicted in Figure 15.
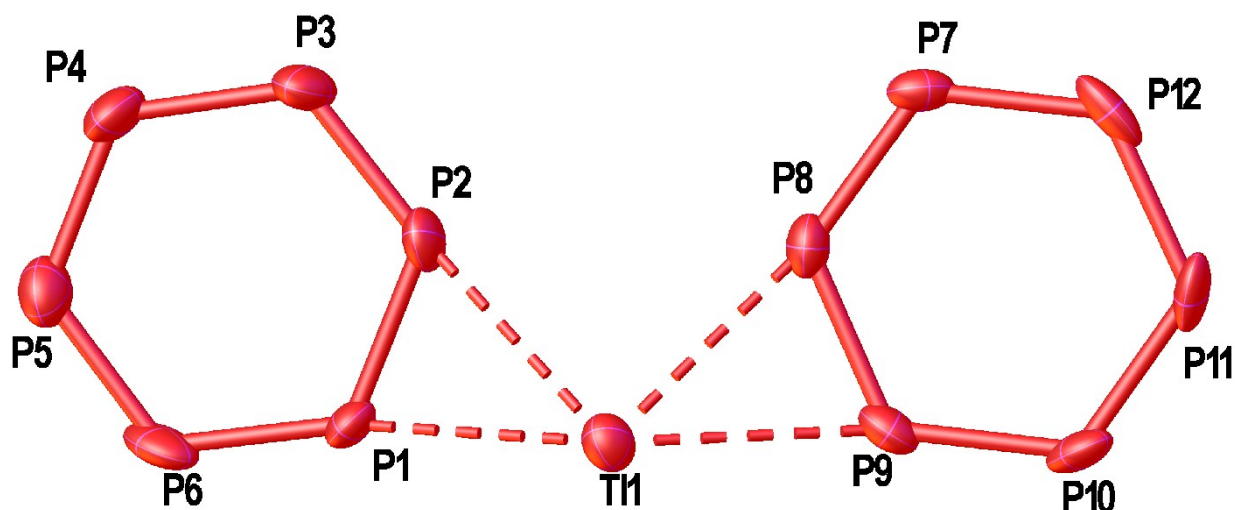
Figure 15. Direct coordination environment of Tl$^+$ in the crystal structure of compound 6 can be described as cationic [Tl(P$_6$)$_2$]$^+$ unit. Cp*Mo fragments are omitted for clarity. Selected bond lengths [Å]: Tl1-P1 3.23284(12), Tl1-P2 3.28516(15), Tl1-P8 3.23938(8), Tl1-P9 3.24129(14).

Tl1 is disordered over a center of inversion and cannot occupy it like Cu$^+$ or Ag$^+$ (see section 6.7, distance Tl1-Tl1' = 4.4448(19) Å). If this is caused by the larger atomic radius of Tl$^+$ or by the tendency to form complexes with a higher coordination number than 2 cannot be further elucidated. Nevertheless, the exchange of the central metal can be done without serious change of the structure type. As a consequence, the *cyclo*-P$_6$ ligand shows two orientations in the solid state with a 1:1 ratio when it is coordinated to Tl1 or Tl1', respectively.[1]
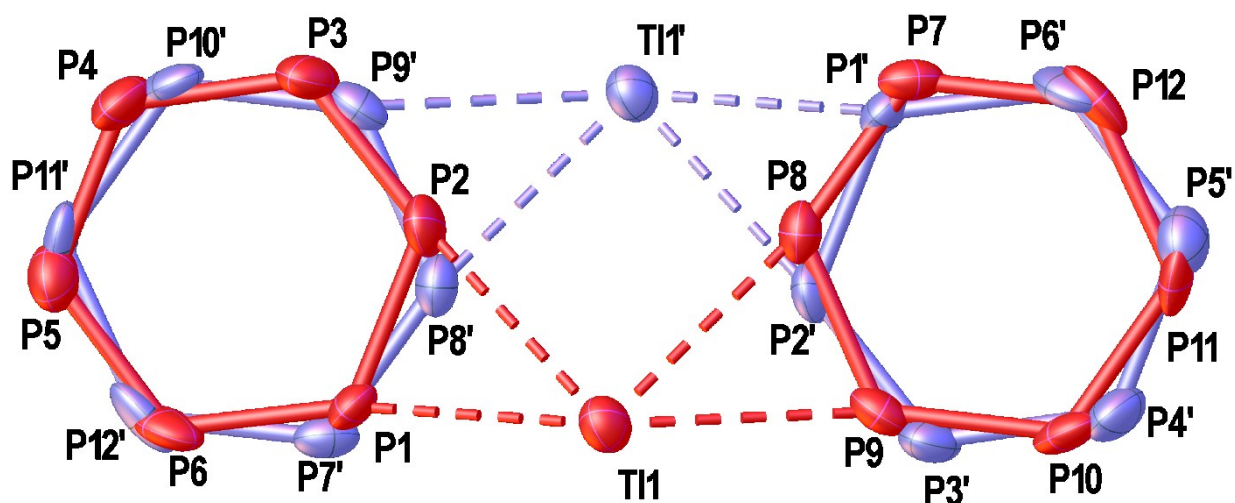
Figure 16. The model of the disorder of the [Tl(P$_6$)$_2$]$^+$ complex over the center of symmetry, where two *cyclo*-P$_6$ ligands in different orientations are coordinated to every Tl cation. Cp*Mo fragments of the P$_6$ ligands are omitted for clarity. A coordination of the Tl cation to the other orientation of the *cyclo*-P$_6$ ligand can be ruled out since it would result in too short Tl-P distances (e.g. Tl1-P8' 2.882 Å vs. Tl1 P2' 3.022 Å).

The present coordination forms [Tl(P$_6$)$_2$]$^+$ coordination units (see Figure 15) with Tl-P distances ranging from ~3.23 – 3.28 Å, but the large Tl$^+$ cation shows also elongated contacts to the P$_6$ rings of the next [Tl(P$_6$)$_2$]$^+$ coordination unit (see Figure 17) which results in a distorted trigonal pyramidal coordination of three P-P bonds to Tl$^+$. The two possible orientations of the third *cyclo*-P$_6$ ligand around Tl$^+$ result in two pairs of Tl-P distances (either Tl1-P5' 3.42008(19), Tl1-P6' 3.69009(11) or Tl1-P12' 3.43(3), Tl1-P11' 3.743(19) which are not shown in Figure 17). These distances are close to each other and therefore no preferred orientation of the third P$_6$ ring can be assumed.

---

(1) A coordination to the other orientation of the cyclo-P6 ligand can be excluded since it would result in too short Tl-P distances which are not in accordance with the weak Tl^I-P interactions present in this compound. (e.g. Tl1-P8' 2.882 Å or Tl1 P2' 3.022 Å).

The crystal packing of **6** (see Figure 18) consists of alternating layers of cationic complexes and negatively charged layers of the [TEF] anions. The 2D cationic layer expands along the crystallographic *bc* plane. The P atoms of all *cyclo*-P_6 ligands of a layer are turned by 14.9°.
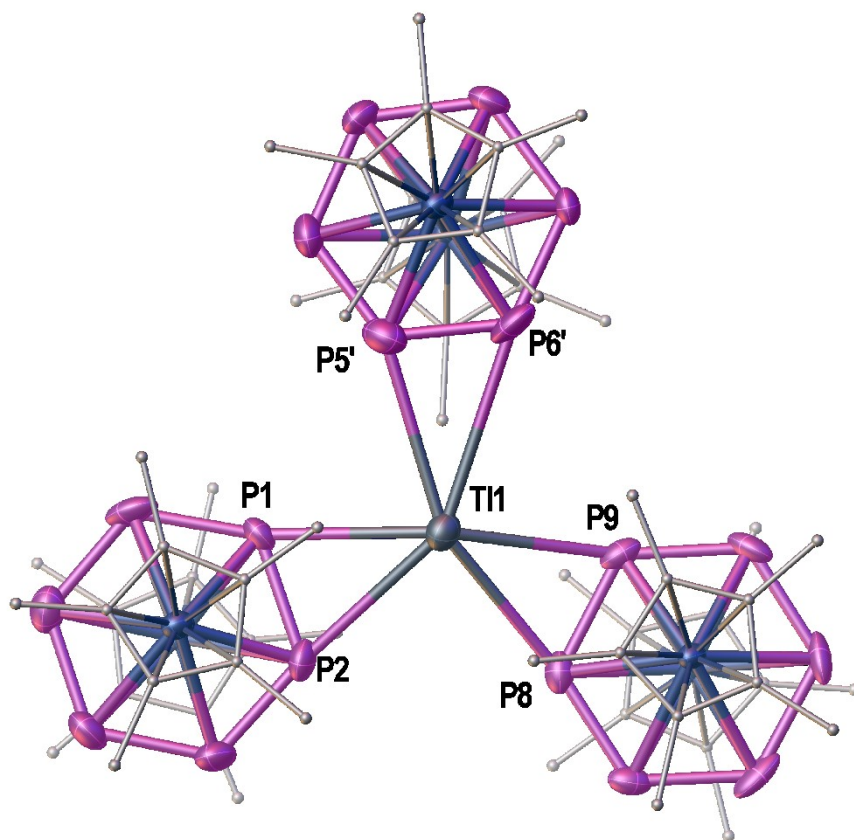
Figure 17. Coordination environment of Tl cation (view along the *a* axis). Selected bond lengths [Å]: Tl1-P1 3.23284(12), Tl1-P2 3.28516(15), Tl1-P8 3.23938(8), Tl1-P9 3.24129(14), Tl1-P5'3.42008(19), Tl1-P6' 3.69009(11), not shown here: Tl1-P12' 3.43(3), Tl1-P11' 3.743(19).
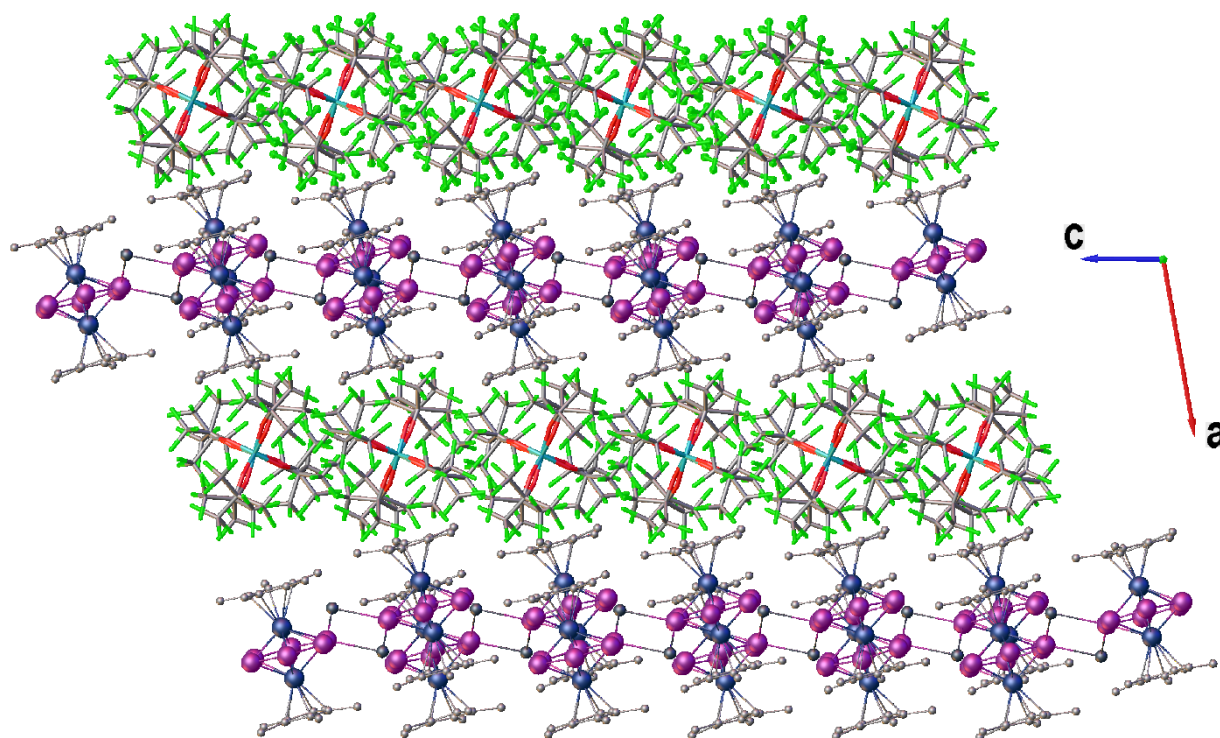
Figure 18. Crystal packing of 6 with viewing direction along the *b*-axis showing alternating layers of the 2D-coordination polymer and the WCAs [TEF].

Figure 19 shows the cationic layer of compound **6** viewed along the crystallographic a axis. Since only Tl1 or Tl1' can be occupied at once (light blue or dark grey, distance Tl-Tl1' = 4.4448(19) Å) and the respective Tl cation is coordinated by an additional *cyclo*-P_6 ligand the resulting assembly, if only one Tl is occupied in an ordered manner (always Tl1 or Tl1'), is presented in Figure 20. The assembly in Figure 20 shows parallel one-dimensional coordination strands of Tl^+ and *cyclo*-P_6 complexes inside the coordination layers. (*This is only one possibility! The Tl cations could also be occupied in a pure statistical manner which would also result in further interconnection of the coordination units. This means that the coordination layers are not completely closed sheets. Additionally this also implies that there would be cavities in the described coordination layers which could be filled by additional metal centers. However, this was unfortunately not possible during this study, since the large anions are necessary in this case to afford a Tl^I coordination to these cyclo-P_6 ligands.*)
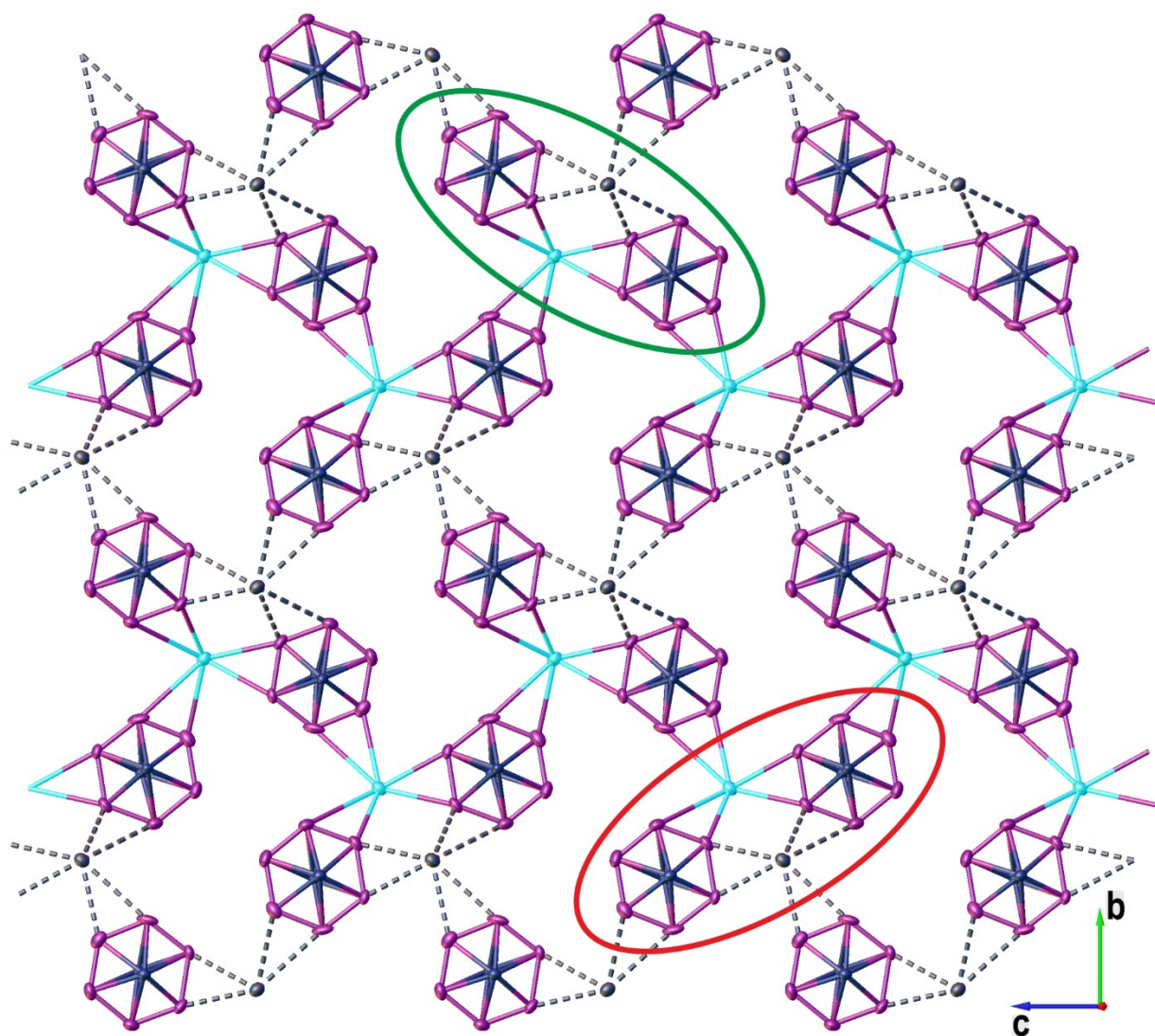
Figure 19. Viewing direction along the crystallographic *a* axis. The half-occupied Tl cations are depicted in dark and light grey and the $[Tl(P_6)_2]^+$ coordination units with shorter Tl-P distances are circumscribed by ellipses. Cp* ligands are omitted for clarity.
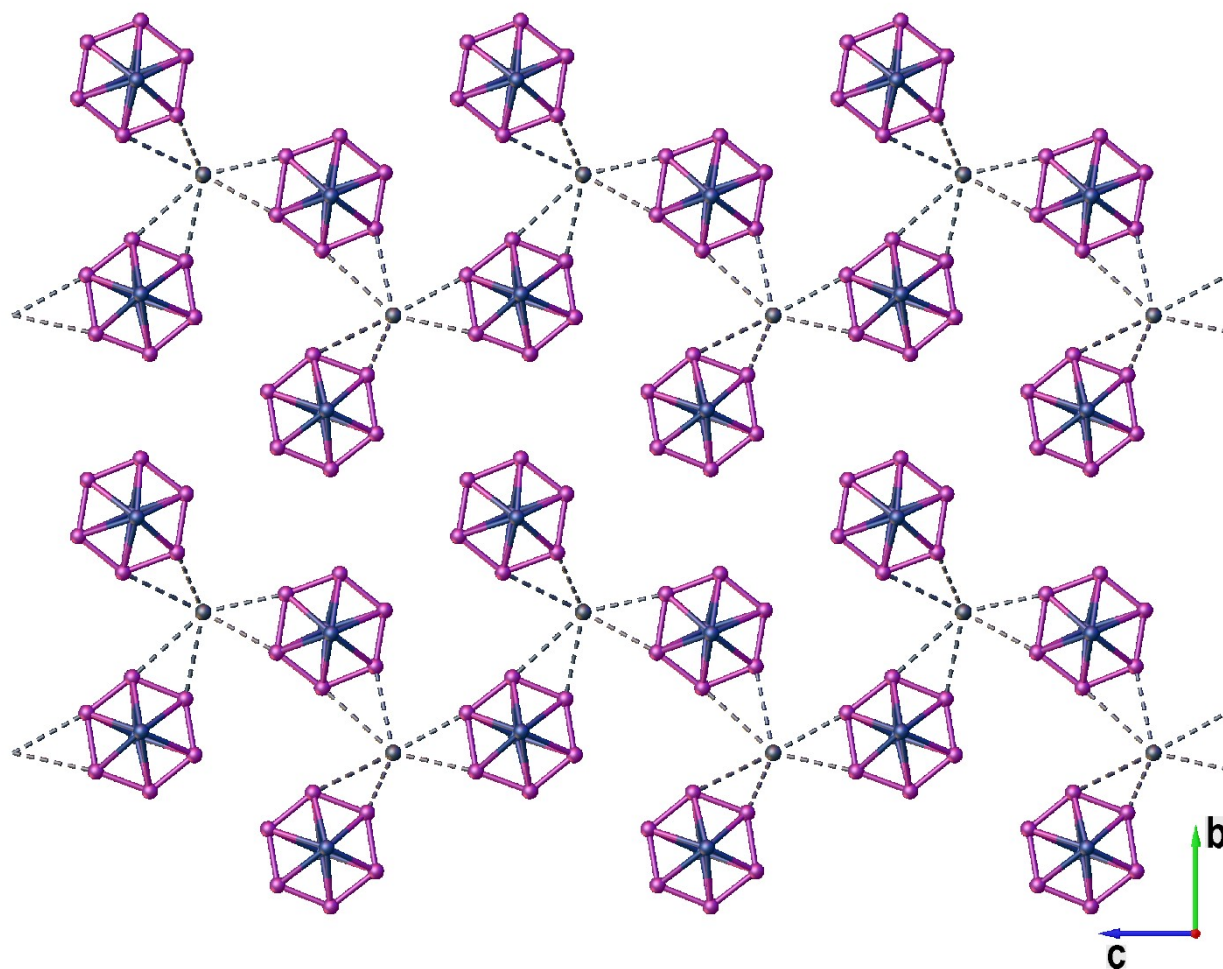
Figure 20. Possible one-dimensional coordination polymer found inside the cationic layers of compound 6 in the solid state. Viewing direction along the *a*-axis.

6.10 Similarity of the crystal structures of 4a, 4b and 6

The compounds **6**, **4a** and **4b** show very similar unit cells and crystallize in the same space group *C*2/*c*. The assembly in the solid state is also very similar with alternating negative layers of the [TEF] anions and positively charged coordination layers along the crystallographic *a* axis shown in Figure 21 c) and d). The similarity of the coordination layers of **6** and **4a-b** are visualized in Figure 21 a) and b). The $[Tl(P_6)_2]^+$ coordination units of **6** (see Figure 15) directly correspond to the complex cations $[M(P_6)_2]^+$ of **4a** (M =Cu, see Figure 13) and **4b** (M = Ag, see Figure 12).
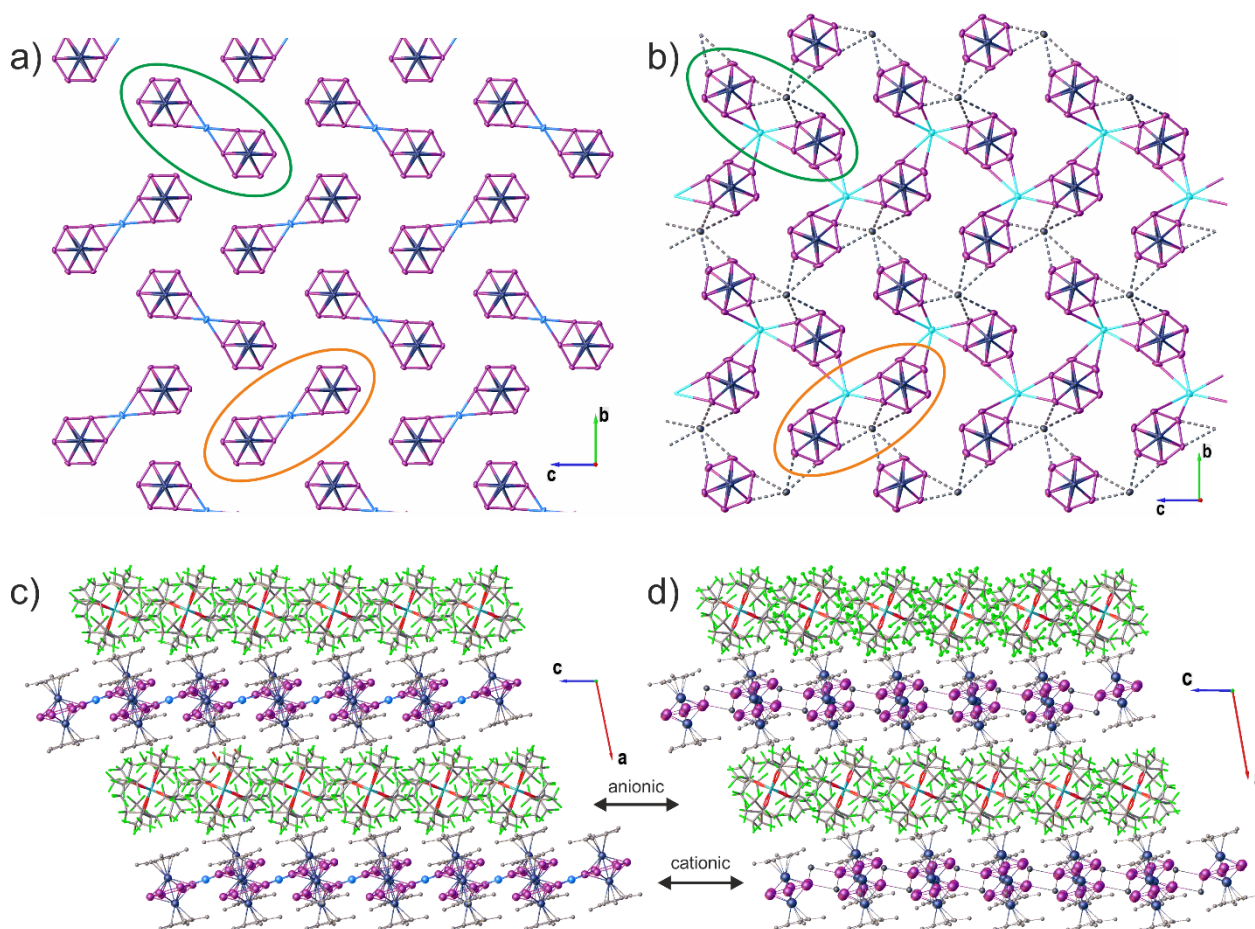
Figure 21. Cationic layers inside the *bc*-plane of 4b a) and 6 b). Tl$^+$ positions (light and dark) in b) are half-occupied. For a) and b) anions, C and H atoms are omitted for clarity. c) + d) Illustration of the crystal packing of 4b c) and 6 d) with viewing direction along the *b*-axis showing the alternation of cationic and anionic layers along the *a*-axis. The P$_6$ planes include a tilt angle of 16.3° (4a), 16.3° (4b) and 13.8° (6) to the *bc*-plane.

7 X-ray powder diffraction analysis

X-ray powder diffraction measurements were carried out with a STOE Stadi P diffractometer with monochromatic Cu-$K_{\alpha 1}$-radiation (λ = 1.540598 Å, Ge-monochromator) and a Mython 1 K detector at 293 K. The 2Θ-range was 2.000° to 93.335° for **4a** and 2.000° to 71.825° for **5**. Diffraction data were analyzed with WINXPOW. The cell constants determined with X-ray powder diffraction at room temperature differs slightly from single crystal data (123 K) and were refined to a = 36.812(9) Å, b = 16.307(6) Å, c = 14.61(2) Å, β = 100.74(3)° and V = 8615(9) Å^3 (**4a**) and a = 16.995(8) Å, b = 17.51(1) Å, c = 19.41(1) Å, α = 109.42(4)°, β = 97.65(4)°, γ = 108.44(3)° and V = 4981(7) Å^3 (**5**), see Table 3. The powder diffraction patterns were simulated with the unit cell parameters which were obtained from the 293 K powder measurement.

Table 3. Refined unit cells of the compounds 4a and 5 by single crystal X-ray diffraction at 123 K and X-ray powder diffraction at 293 K.

	4a		5	
	single crystal (123 K)	powder (293 K)	single crystal (123 K)	powder (293 K)
a [Å]	36.4679(6)	36.812(9)	16.7510(5)	16.995(8)
b [Å]	16.1466(3)	16.307(6)	17.2703(7)	17.51(1)
c [Å]	14.4134(2)	14.61(2)	18.8355(6)	19.41(1)
α [°]	90	90	109.136(3)	109.42(4)
β [°]	101.863(2)	100.74(3)	97.750(3)	97.65(4)
γ [°]	90	90	108.799(3)	108.44(3)
V [Å^3]	8305.8(2)	8615(9)	4693.8(3)	4981(7)
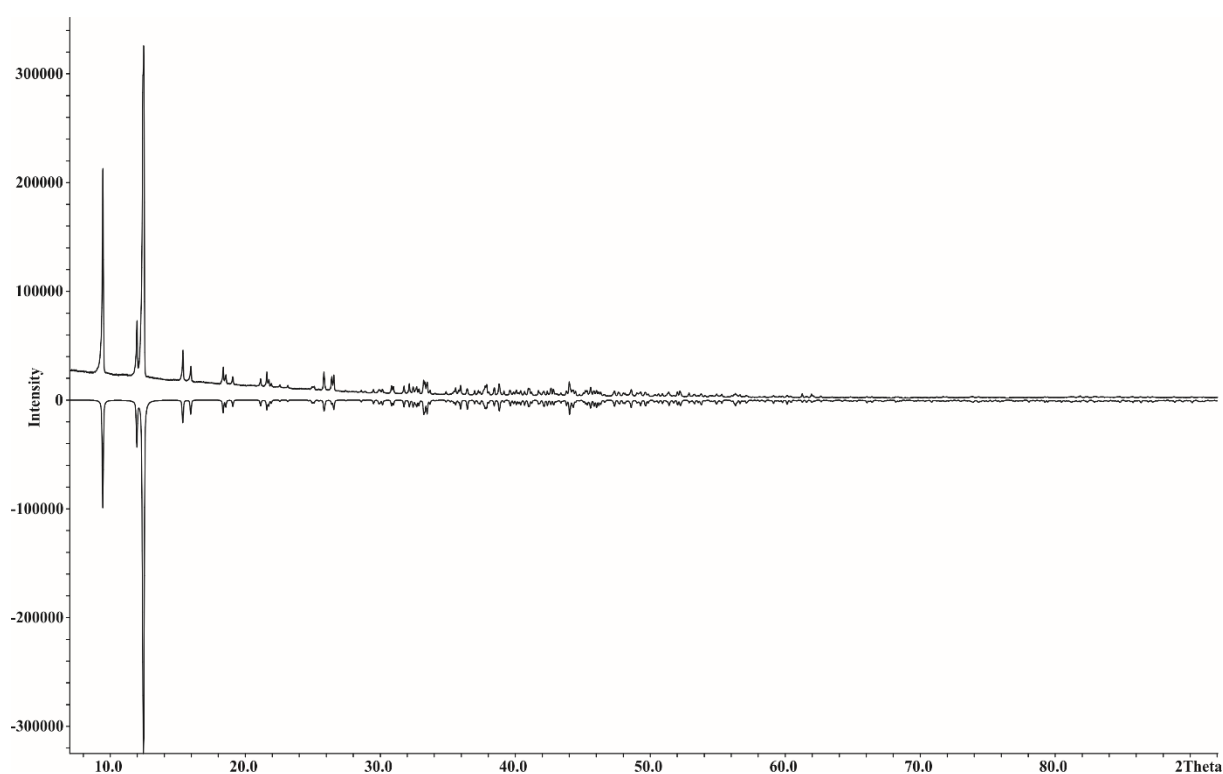
Figure 22. X-ray powder pattern for the pure *cyclo*-P$_6$ complex 1. Positive intensities (measured), negative intensities (simulated).
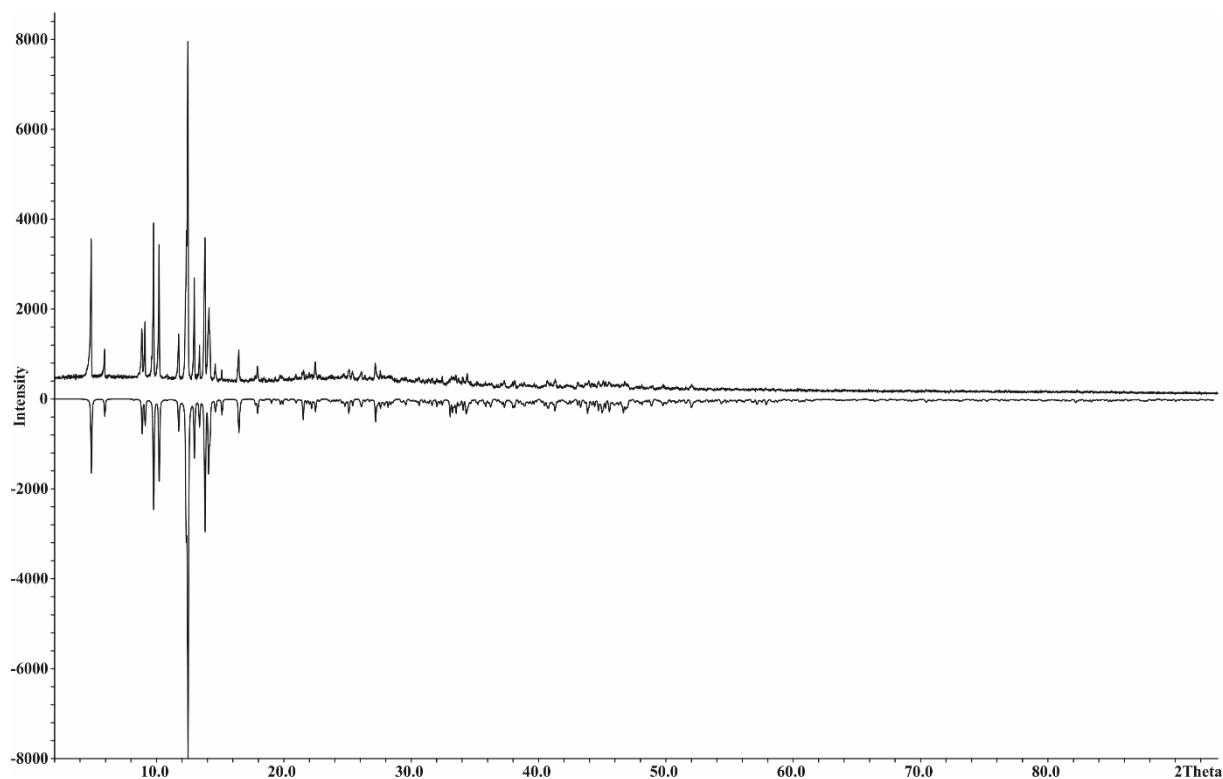
Figure 23. X-ray diffraction pattern for compound 4a. Positive intensities (measured), negative intensities (simulated).
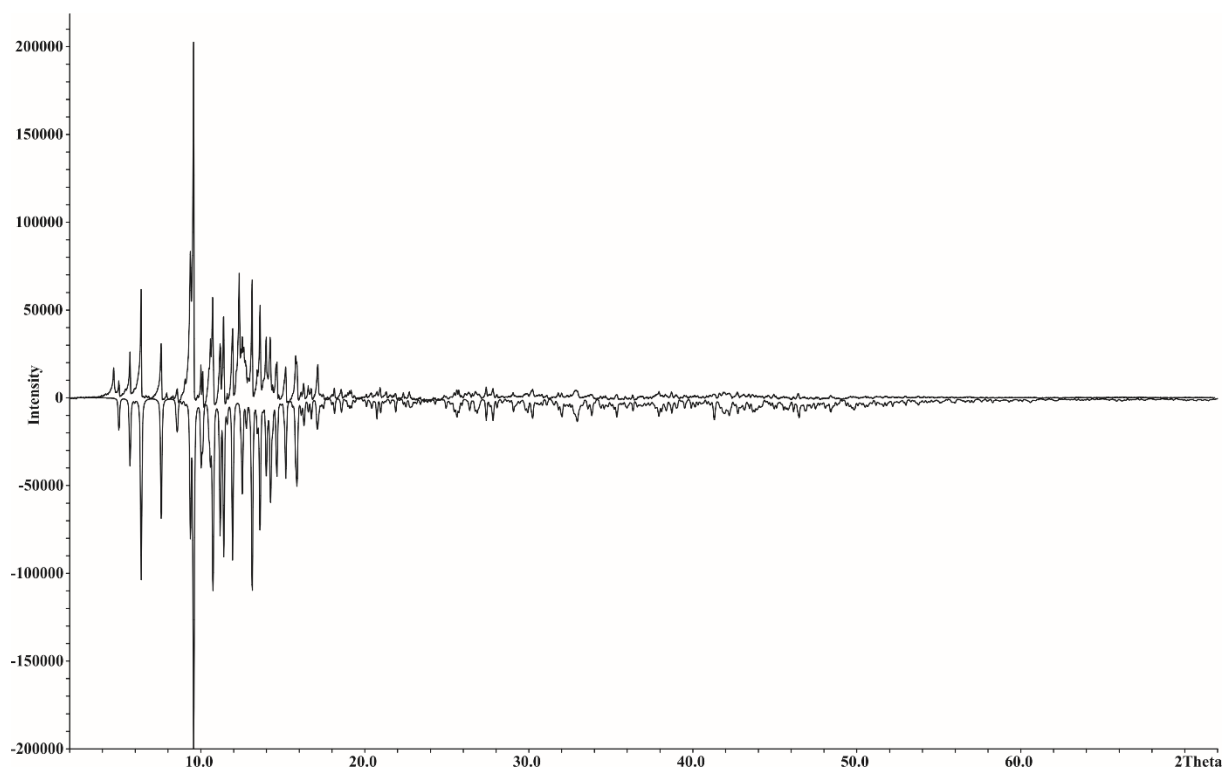
Figure 24. Xray powder diffraction pattern for compound 5. Positive intensities (measured), negative intensities (simulated).

8 DFT calculation

8.1 DFT calculations for [(Cp*Mo)$_2$(μ-P$_{10}$)] (2)

All calculations have been performed with the TURBOMOLE program package[12]. For the analysis of the bonding situation in [(Cp*Mo)$_2$(P$_{10}$)] the BP86 functional together with the def2-TZVP basis set has been used. The reaction energies has been calculated at the B3LYP[13]/def2-TZVP[14] level of theory. The nature of the stationary point was checked by calculating the vibration frequencies. All complexes show no negative frequencies, except [(Cp*Mo)$_2$(P$_{10}$)] for which one negative frequency (5.24 cm^{-1}) corresponding to the rotation of the Cp* ligand was observed. Repeated geometry optimizations did not lead to the elimination of this negative frequency. For calculating the reaction energies, this negative frequency has been ignored. The reported population analysis[15] was performed as implemented in TURBOMOLE.

The reaction energy of the transformation [(Cp*Mo)$_2$(P$_{10}$)] $\rightarrow$ [(Cp*Mo)$_2$(P$_6$)] + P$_4$ is -19.64 kJ·mol^{-1} (corrected for zero point vibration energy; -13.26 kJ·mol^{-1} not corrected)

LMO 155   LMO 145   LMO 146   LMO 156
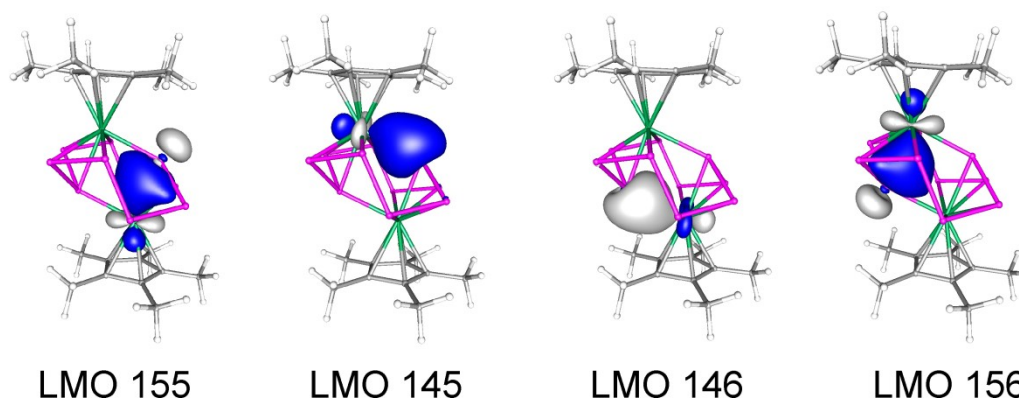
Figure 25. Isosurfaces of Localized Molecular Orbitals (LMO) representing the Mo-P bonding interactions, calculated at the BP86/def2-TZVP level of theory.
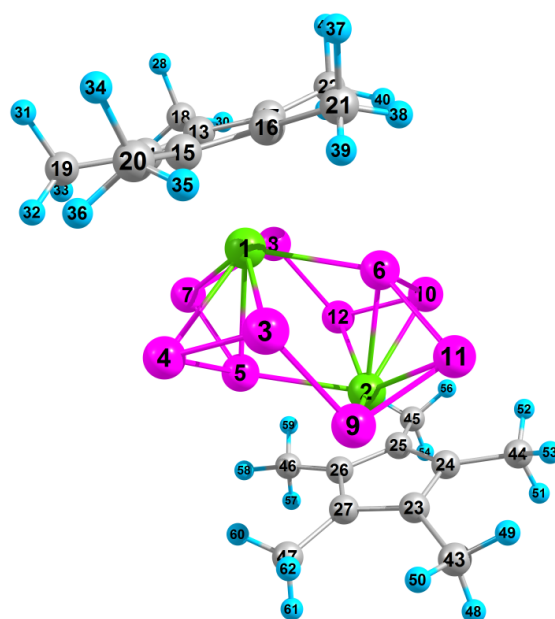
Figure 26. Atom labeling in [(Cp*Mo)$_2$(μ-P$_{10}$)].

Table 4. Wiberg Bond Indices (WBI) of selected bonds in [(Cp*Mo)₂(μ-P₁₀)], calculated at the BP86/def2-TZVP level of theory. Labeling according to Figure 26.

Bond	WBI	Bond	WBI	Bond	WBI
mo 2 - mo 1	0.16	p 7 - mo 1	0.85	p 10 - mo 2	0.85
p 3 - mo 1	0.86	p 7 - p 3	0.04	p 10 - p 6	0.94
p 4 - mo 1	0.85	p 7 - p 4	0.05	p 11 - mo 2	0.85
p 4 - p 3	1.10	p 7 - p 5	0.94	p 11 - p 6	0.94
p 5 - mo 1	0.76	p 8 - mo 1	0.86	p 11 - p 9	1.10
p 5 - mo 2	0.70	p 8 - p 7	1.10	p 11 - p 10	0.05
p 5 - p 4	0.94	p 9 - mo 2	0.86	p 12 - mo 2	0.86
p 6 - mo 1	0.70	p 9 - p 3	1.03	p 12 - p 8	1.03
p 6 - mo 2	0.76	p 9 - p 4	0.04	p 12 - p 10	1.10

Table 5. Cartesian coordinates of the optimized geometry of [(Cp*Mo)₂(μ-P₁₀)], at the B3LYP/def2-TZVP level of theory. Total energy -4329.879804523 Hartree; ZPE = 0.4656262 ha.

Atom	x	y	z
Mo	−0.1554164	1.3814617	1.2799615
Mo	0.1553810	−1.3813960	−1.2799801
P	−0.5435910	−0.8635584	2.4998552
P	−2.3084751	0.1537025	1.8263903
P	−1.6598348	0.0999057	−0.2867362
P	1.6598079	−0.0997873	0.2866292
P	−1.7898894	2.3025281	−0.4298684
P	0.2653441	2.4863136	−1.0170745
P	−0.2652971	−2.4862428	1.0170793
P	2.3083345	−0.1536092	−1.8265127
P	1.7899207	−2.3023955	0.4298124
P	0.5434592	0.8636738	−2.4999378
C	0.3597556	3.6523345	1.9525385
C	−0.6158234	3.1402433	2.8570566
C	−0.0083550	2.0833624	3.5961229
C	1.3316308	1.9174037	3.1242359
C	1.5599503	2.8896708	2.1067152
C	0.2221357	4.9246325	1.1775543
C	−1.9576069	3.7443095	3.1331047
C	−0.5929250	1.4495894	4.8189393
C	2.3634097	1.0166270	3.7282127
C	2.8741095	3.1910615	1.4564063
C	−0.3597679	−3.6523230	−1.9524987
C	0.6158210	−3.1402342	−2.8569992
C	0.0083753	−2.0833584	−3.5960855
C	−1.3316272	−1.9174096	−3.1242492
C	−1.5599672	−2.8896797	−2.1067163
H	0.4563844	5.7711416	1.8323087
H	−0.7920426	5.0688040	0.8050334
H	0.8969909	4.9633077	0.3251758
H	−1.8719843	4.5269111	3.8951630
H	−2.6650691	3.0009514	3.4976482
H	−2.3861243	4.1957069	2.2394332
H	−0.4089497	2.0984107	5.6822805
H	−0.1523463	0.4775892	5.0299493
H	−1.6711553	1.3142363	4.7340065
H	2.8482839	1.5139024	4.5749334
H	3.1402360	0.7545925	3.0110470
H	1.9230064	0.0895479	4.0937069
H	3.5035561	2.3048016	1.3862167

```
H     3.4199878      3.9392858      2.0408162
H     2.7435917      3.5854049      0.4491774
C    -0.2221530     -4.9246488     -1.1775634
C     1.9576385     -3.7442766     -3.1329759
C     0.5929585     -1.4496763     -4.8189410
C    -2.3634027     -1.0166653     -3.7282627
C    -2.8741184     -3.1910730     -1.4564023
H    -0.4563634     -5.7711430     -1.8323516
H     0.7920214     -5.0688119     -0.8050224
H    -0.8970252     -4.9633688     -0.3252093
H     1.8720778     -4.5269062     -3.8950170
H     2.6650946     -3.0008999     -3.4975037
H     2.3861362     -4.1956352     -2.2392718
H     0.4090107     -2.0985728     -5.6822307
H     0.1523626     -0.4777077     -5.0300426
H     1.6711869     -1.3142949     -4.7340032
H    -2.8482358     -1.5139682     -4.5749788
H    -3.1402430     -0.7546464     -3.0111288
H    -1.9230254     -0.0895864     -4.0937602
H    -3.5035803     -2.3048424     -1.3862354
H    -3.4199775     -3.9393230     -2.0407812
H    -2.7435867     -3.5853728     -0.4491703
```

8.2   DFT calculations for $[(Cp*Mo)_2(\mu\text{-}\eta^6{:}\eta^6\text{-}P_6)]^{0/+}$ (1, 3a, 3b)

All calculations have been performed with the TURBOMOLE program package[12] at the RI-[16]BP86[13]/def2-TZVP[14] level of theory, followed by single point calculations without the RI approximation. The Multipole Accelerated Resolution of Identity (MARI-J)[17] approximation was used in the geometry optimization steps. The nature of the stationary point was checked by the frequency calculations. For $[(Cp*Mo)_2(P_6)]$ a negative frequency of -2.26 cm^{-1} corresponding to the rotation of the Cp* ligand was observed. Although the geometry has been optimized repeatedly using different methods and different input geometries, this negative frequency persisted.

The inspection of the frontier molecular orbitals in $[(Cp*Mo)_2(\mu,\eta^6{:}\eta^6\text{-}P_6)]$ (1) shows, that the HOMO and HOMO-1 orbitals are basically degenerate and represent P-P bonding with contribution of molybdenum d orbitals. By elimination of one electron the HOMO-1 orbital in 1 is converted to the Single Occupied Molecular Orbital (SOMO) in [1]$^+$ (Figure 27 and Figure 28). This leads to the reduction of the P-P bond order (two opposite P-P bonds) and to the observed bis-allylic distortion. This behavior is also nicely described by the Wiberg Bond Indices. The WBI for all P-P bonds in 1 is the same and equals to 0.86 whereas in [1]$^+$ the WBI corresponding to the elongated P-P bonds are 0.67 and while it is 0.95 for the other P-P bonds. The WBI for the Mo-Mo bond (2.669 Å and 2.698 Å in 1 and [1]$^+$, respectively) is 0.86 in 1 and 0.95 in 1$^+$.

LUMO (-1.960 eV)   HOMO (-4.266 eV)   HOMO-1 (-4.267 eV)   HOMO-2 (-5.134 eV)
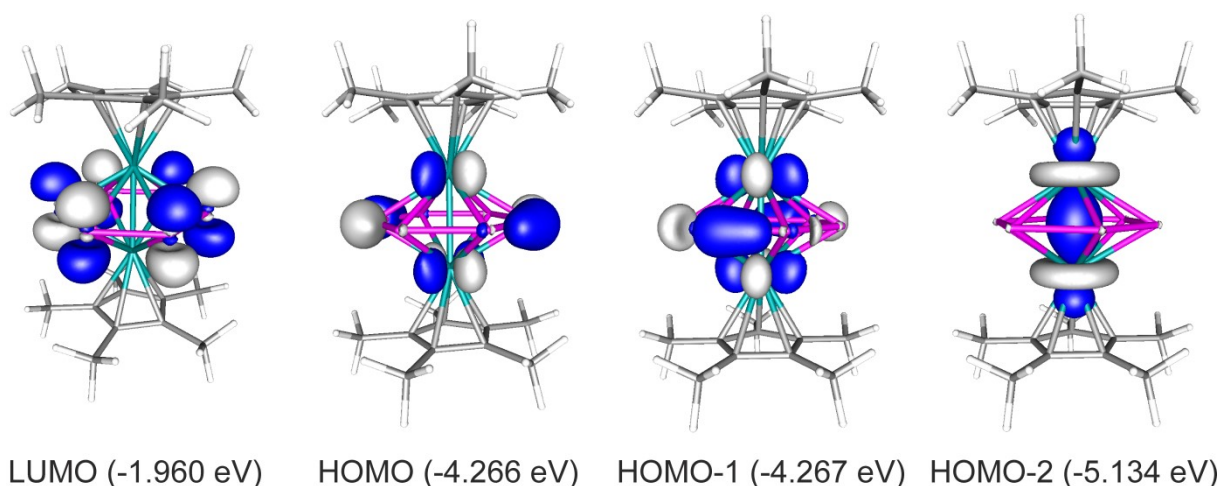
Figure 27. Isosurfaces of selected molecular orbitals in [(Cp*Mo)$_2$(μ,η^6:η^6-P$_6$)] (1). Calculated at the BP86/def2-TZVP level of theory.

LUMO (-5.597 eV)   SOMO (-7.769 eV)   HOMO-1 (-8.393 eV)   HOMO-2 (-8.772 eV)
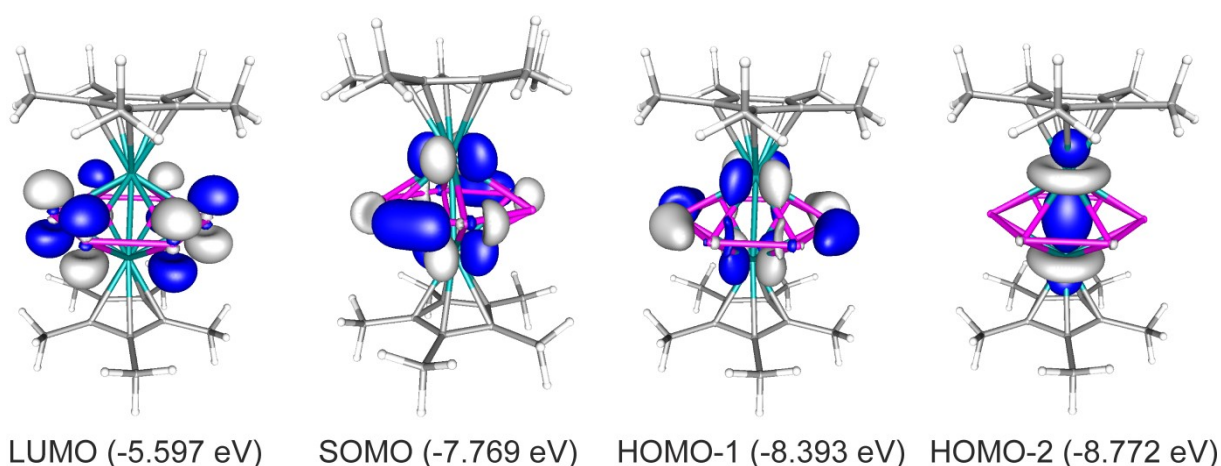
Figure 28. Isosurfaces of selected molecular orbitals in [(Cp*Mo)$_2$(μ,η^6:η^6-P$_6$)]$^+$ (= [1]$^+$). Calculated at the BP86/def2-TZVP level of theory.

Table 6. Cartesian coordinates of the optimized geometry of [(Cp*Mo)$_2$(μ,η^6:η^6-P$_6$)] (1) at the BP86/def2-TZVP level of theory. Total energy: -2965.97388640914 a.u.

Atom	x	y	z
Mo	−0.3419705	−0.6113511	−1.1358570
Mo	0.3419809	0.6113571	1.1358589
P	−1.7434335	−0.8979771	1.0024832
P	1.7434482	0.8979791	−1.0025021
P	1.9312947	−1.0590914	−0.0092943
P	−1.9312757	1.0590996	0.0092692
P	0.1884327	−1.9565342	0.9942329
P	−0.1884093	1.9565357	−0.9942551
C	−1.8058178	−2.0510450	−2.3003763
C	−0.4823735	−0.5491063	−3.4874587
C	−1.8068061	−0.7816786	−2.9772876
C	−0.4802608	−2.6024891	−2.3925374
C	0.3372291	−1.6739367	−3.1260194
C	1.8058216	2.0510473	2.3003937
C	0.4823649	0.5491037	3.4874563
C	1.8068030	0.7816782	2.9772986
C	0.4802643	2.6024918	2.3925437
C	−0.3372341	1.6739371	3.1260144

```
C    -3.0097452   -2.7508384   -1.7453846
C    -0.0674247    0.5855920   -4.3737986
C    -3.0088339    0.0720040   -3.2482295
C    -0.0626886   -3.9717626   -1.9481854
C     1.7495934   -1.9047713   -3.5700062
C     3.0097529    2.7508400    1.7454100
C     0.0674076   -0.5855982    4.3737868
C     3.0088276   -0.0720072    3.2482437
C     0.0626981    3.9717657    1.9481883
C    -1.7496022    1.9047708    3.5699871
H    -2.7462023   -3.4133552   -0.9110983
H    -3.4888971   -3.3679502   -2.5241839
H    -3.7592368   -2.0386093   -1.3775958
H    -0.6553199    1.4908536   -4.1752103
H    -0.2105489    0.3185936   -5.4343405
H     0.9908050    0.8427573   -4.2347478
H    -3.7733272   -0.0445428   -2.4696820
H    -3.4681180   -0.2048896   -4.2121772
H    -2.7480258    1.1371368   -3.2979282
H     0.9930293   -3.9969378   -1.6483975
H    -0.1954646   -4.6992232   -2.7666234
H    -0.6567382   -4.3195169   -1.0935050
H     2.3069486   -0.9624711   -3.6520312
H     1.7687110   -2.3929685   -4.5587953
H     2.2942026   -2.5496485   -2.8683837
H     2.7462155    3.4133579    0.9111211
H     3.4889001    3.3679532    2.5242123
H     3.7592484    2.0386097    1.3776276
H     0.6553098   -1.4908581    4.1752035
H     0.2105181   -0.3186023    5.4343323
H    -0.9908211   -0.8427654    4.2347214
H     3.7733270    0.0445449    2.4697009
H     3.4681073    0.2048808    4.2121961
H     2.7480176   -1.1371413    3.2979352
H    -0.9930179    3.9969420    1.6483891
H     0.1954667    4.6992267    2.7666282
H     0.6567593    4.3195204    1.0935143
H    -2.3069608    0.9624701    3.6520000
H    -1.7687288    2.3929618    4.5587805
H    -2.2942022    2.5496566    2.8683632
```

Table 7. Cartesian coordinates of the optimized geometry of [(Cp*Mo)₂(μ,η^6:η^6-P₆)]⁺ (= [1]⁺) at the BP86/def2-TZVP level of theory. Total energy: -2965.75991466951 a.u.

Atom	x	y	z
Mo	0.0628240	0.0068417	-1.3475161
Mo	-0.0627828	0.0068731	1.3475261
P	2.2781204	0.0067629	0.1046151
P	-1.1465185	-1.8263983	-0.0519658
P	1.1469230	-1.8261798	0.0521133
P	-2.2781136	0.0063003	-0.1046897
P	-1.1465093	1.8389031	-0.0522379
P	1.1461729	1.8391585	0.0521860
C	1.3508012	-0.2406170	-3.3149865
C	0.7523160	1.0697005	-3.3437348
C	0.2939881	-1.2160129	-3.3610344
C	2.8160176	-0.5382908	-3.4109153
C	-0.6748805	0.9032915	-3.4034165
C	1.4899030	2.3671194	-3.4731877
C	-0.9578946	-0.5101534	-3.4125942
C	-1.6788676	1.9965456	-3.6044996
C	-2.3035777	-1.1335916	-3.6220784
C	0.4708031	-2.6966847	-3.5000550

```
H     3.0755808   -1.4896871   -2.9299026
H     3.4288523    0.2508882   -2.9577538
H     3.1111465   -0.6150925   -4.4700473
H     1.6678414    2.5906215   -4.5376304
H     2.4682824    2.3372238   -2.9774814
H     0.9228554    3.2064674   -3.0518425
H    -2.4887225   -1.2685564   -4.6999997
H    -3.1135483   -0.5077806   -3.2267543
H    -2.3767954   -2.1215564   -3.1503343
H    -0.3748001   -3.2527204   -3.0762231
H     1.3871012   -3.0492248   -3.0104657
H     0.5417316   -2.9668342   -4.5661260
H    -1.3473692    2.9453678   -3.1648454
H    -2.6547210    1.7448920   -3.1705025
H    -1.8329424    2.1685359   -4.6820661
C    -1.3508149   -0.2405856    3.3149911
C    -0.7522988    1.0697164    3.3437561
C     0.6748926    0.9032709    3.4034396
C     0.9578734   -0.5101779    3.4125966
C    -0.2940251   -1.2160058    3.3610324
C    -2.8160387   -0.5382263    3.4108914
C    -1.4898508    2.3671555    3.4732015
C     1.6789086    1.9964980    3.6045237
C     2.3035442   -1.1336464    3.6220726
C    -0.4708679   -2.6966751    3.5000359
H    -3.0756146   -1.4896136    2.9298769
H    -3.4288457    0.2509672    2.9577279
H    -3.1111878   -0.6150255    4.4700161
H    -1.6677438    2.5906953    4.5376414
H    -2.4682469    2.3372685    2.9775371
H    -0.9228011    3.2064768    3.0518142
H     1.3474225    2.9453345    3.1648982
H     2.6547426    1.7448306    3.1704967
H     1.8330176    2.1684658    4.6820871
H     2.4887052   -1.2686040    4.6999906
H     3.1135236   -0.5078629    3.2267277
H     2.3767318   -2.1216160    3.1503398
H     0.3747104   -3.2527209    3.0761740
H    -1.3871854   -3.0491927    3.0104743
H    -0.5417684   -2.9668391    4.5661034
```

8.3 DFT calculations for the equilibria of square planar and tetrahedral isomers of the complex cations $[M(1)_2]^+$ M = Cu, Ag

The geometries of the compounds have been fully optimized with gradient-corrected density functional theory (DFT) in form of Becke's three-parameter hybrid method B3LYP[18] with def2-SVP all electron basis set (ECP on Mo,Ag).[19] Gaussian 03 program package[20] was used throughout. All structures correspond to minima on their respective potential energy surfaces. Solvent effects have been estimated by performing single point energy computation of gas-phase optimized geometries using polarisable continuum model (PCM) as implemented in Gaussian 03.

For Cu compounds, optimization of a planar isomer in framework of C_i point group (inversion center) resulted in transition state structure, which is only by 0.7 kJ mol^{-1} higher than asymmetric minimum. Planar isomer is predicted to be energetically less stable than tetrahedral (24.6 kJ mol^{-1} in the gas phase), but has larger standard entropy. Values for the equilibrium constant for the isomerization reaction *tetrahedral → square planar* are 0.12, 0.24, and 0.38 for the gas phase, toluene and dichloromethane solutions, respectively. Thus, from the thermodynamic point of view, both isomers should be present in solution at room temperature (with tetrahedral isomer having the higher concentration). The influence of the solvent on the energetic of isomerization processes is rather small.

However, changing from the gas phase to toluene and dichloromethane solutions increases concentration of the less stable planar isomer, but tetrahedral one remains dominant in all cases.

For Ag analogs, energetically the tetrahedral isomer is also more stable, but the difference is only 9.5 kJ mol^{-1} in the gas phase and 6.0 and 4.2 kJ mol^{-1} in toluene and dichloromethane. Due to entropy factor, planar isomer is predicted to be dominant in solution: values for the equilibrium constant for the isomerization reaction *tetrahedral* $\rightarrow$ *square planar* are 7.0, 28.3, and 59.1 for the gas phase, toluene and dichloromethane solutions, respectively. Thus, molar fraction of tetrahedral isomer with respect to planar is predicted to be below 4% in toluene and below 2% in dichloromethane. Thus, planar isomer should be dominant in solution.

Table 8. Total energies E^o_0, PCM energies for toluene and dichloromethane solutions, E^o_0 (toluene) and E^o_0 (CH$_2$Cl$_2$), sum of electronic and thermal enthalpies H^o_{298} (all in Hartree) and standard entropies S^o_{298} (cal mol^{-1}K^{-1}) for studied compounds. B3LYP/def2-SVP (ECP on Mo,Ag) level of theory.

compound	E^o_0	E^o_0 (toluene)	E^o_0 (CH$_2$Cl$_2$)	H^o_{298}	S^o_{298}
Cu_planar (**4a**)	-7568.108574	-7568.133853	-7568.147889	-7567.115046	397.466
Cu_tetrahedral (**5**)	-7568.117955	-7568.142554	-7568.156147	-7567.123604	383.732
Ag_planar (**4b**)	-6074.775007	-6074.801541	-6074.817175	-6073.781725	406.935
Ag_tetrahedral	-6074.778622	-6074.803836	-6074.818774	-6073.784875	396.442

Table 9. Reaction energies ΔE^o_0, standard enthalpies ΔH^o_{298} and Gibbs energies ΔG^o_{298} (kJ mol^{-1}), standard entropies ΔS^o_{298} (J mol^{-1}K^{-1}) and equilibrium constants K_{298} for the isomerization process *tetrahedral* $\rightarrow$ *square planar* in different media. Energetic data in dichloromethane and toluene solutions are computed as single point energy calculations on gas phase optimized geometries in polarized continuum model (PCM) approximation. B3LYP/def2-SVP (ECP on Mo, Ag) level of theory.

compound	medium	ΔE^o_0	ΔH^o_{298}	ΔS^o_{298}	ΔG^o_{298}	K_{298}
Cu	gas phase	24.6	22.5	57.5	5.34	0.12
	toluene	22.8	20.7	57.5	3.55	0.24
	DCM	21.7	19.5	57.5	2.39	0.38
Ag	gas phase	9.5	8.3	43.9	-4.8	7.0
	toluene	6.0	4.8	43.9	-8.3	28.3
	DCM	4.2	3.0	43.9	-10.1	59.1

[1]   R. B. King, M. Z. Iqbal, A. D. King Jr, *J. Organomet. Chem.* **1979**, *171*, 53-63.
[2]   I. Krossing, *Chem. Eur. J.* **2001**, *7*, 490-502.
[3]   T. Köchner, N. Trapp, T. A. Engesser, A. J. Lehner, C. Röhr, S. Riedel, C. Knapp, H. Scherer, I. Krossing, *Angew. Chem. Int. Ed.* **2011**, *50*, 11253-11256; *Angew. Chem.* **2011**, *123*, 11449-11452.
[4]   G. Santiso-Quiñones, A. Higelin, J. Schaefer, R. Brückner, C. Knapp, I. Krossing, *Chem. Eur. J.* **2009**, *15*, 6663-6677.
[5]   M. Gonsior, I. Krossing, N. Mitzel, *Z. Anorg. Allg. Chem.* **2002**, *628*, 1821-1830.
[6]   O. J. Scherer, H. Sitzmann, G. Wolmershäuser, *Angew. Chem. Int. Ed.* **1985**, *24*, 351-353; *Angew. Chem.* **1985**, *97*, 358-359.
[7]   D. F. Evans, *J. Chem. Soc.* **1959**, 2003-2005.
[8]   D. F. Evans, G. V. Fazakerley, R. F. Phillips, *J. Chem. Soc. A* **1971**, 1931-1934.
[9]   T. H. Crawford, J. Swanson, *J. Chem. Educ.* **1971**, *48*, 382.
[10]   D. H. Grant, *J. Chem. Educ.* **1995**, *72*, 39.
[11]   G. J. P. Britovsek, V. C. Gibson, S. K. Spitzmesser, K. P. Tellmann, A. J. P. White, D. J. Williams, *J. Chem. Soc., Dalton Trans.* **2002**, 1159-1171.
[12]   a) R. Ahlrichs, M. Bär, M. Häser, H. Horn, C. Kölmel, *Chem. Phys. Lett.* **1989**, *162*, 165–169; b) O. Treutler, R. Ahlrichs, *J. Chem. Phys.* **1995**, *102*, 346–354.
[13]   a) P. A. M. Dirac, *Proc. Royal Soc.A*, **1929**, *123*, 714. b) J. C. Slater, *Phys. Rev.* **1951**, *81*, 385. c) S. H. Vosko, L. Wilk, M. Nusair, *Can. J. Phys.* **1980**, *58*, 1200. d) A. D. Becke, *Phys. Rev. A*, **1988**, *38*, 3098. e) C. Lee, W. Yang, R. G. Parr, *Phys. Rev. B*, **1988**, *37*, 785. f) A. D. Becke, *J. Chem. Phys.* **1993**, *98*, 5648.
[14]   a) A. Schäfer, C. Huber, R. Ahlrichs, *J. Chem. Phys.* **1994**, *100*, 5829; b) K. Eichkorn, F. Weigend, O. Treutler, R. Ahlrichs, *Theor. Chem. Acc.* **1997**, *97*, 119.
[15]   A. E. Reed, R. B. Weinstock, F. Weinhold, *J. Chem. Phys.*, **1985**, *83*, 735-746.
[16]   a) K. Eichkorn, O. Treutler, H. Oehm, M. Häser, R. Ahlrichs, *Chem. Phys. Lett.* **1995**, *242*, 652–660; b) K. Eichkorn, F. Weigend, O. Treutler, R. Ahlrichs, *Theor. Chem. Acc.* **1997**, *97*, 119.

[17] M. Sierka, A. Hogekamp, R. Ahlrichs, *J. Chem. Phys.* 2003, **118**, 9136.

[18] a) A.D. Becke, *J. Chem. Phys.* **1993**, *98*, 5648. b) C. Lee, W. Yang, R.G. Parr, *Phys. Rev. B.* **1988**, *37*, 785.

[19] a) F. Weigend, R. Ahlrichs, *Phys.Chem.Chem.Phys.*, **2005**, *7*, 3297-3305. b) D. Andrae, U. Haeussermann, M.Dolg, H.Stoll, H.Preuss, *Theor.Chim.Acta,* **1990**, *77*, 123-141. .

[20] M. J. Frisch, G. W. Trucks, H. B. Schlegel, G. E. Scuseria, M. A. Robb, J. R. Cheeseman, J. A. Montgomery, Jr., T. Vreven, K. N. Kudin, J. C. Burant, J. M. Millam, S. S. Iyengar, J. Tomasi, V. Barone, B. Mennucci, M. Cossi, G. Scalmani, N. Rega, G. A. Petersson, H. Nakatsuji, M. Hada, M. Ehara, K. Toyota, R. Fukuda, J. Hasegawa, M. Ishida, T. Nakajima, Y. Honda, O. Kitao, H. Nakai, M. Klene, X. Li, J. E. Knox, H. P. Hratchian, J. B. Cross, V. Bakken, C. Adamo, J. Jaramillo, R. Gomperts, R. E. Stratmann, O. Yazyev, A. J. Austin, R. Cammi, C. Pomelli, J. W. Ochterski, P. Y. Ayala, K. Morokuma, G. A. Voth, P. Salvador, J. J. Dannenberg, V. G. Zakrzewski, S. Dapprich, A. D. Daniels, M. C. Strain, O. Farkas, D. K. Malick, A. D. Rabuck, K. Raghavachari, J. B. Foresman, J. V. Ortiz, Q. Cui, A. G. Baboul, S. Clifford, J. Cioslowski, B. B. Stefanov, G. Liu, A. Liashenko, P. Piskorz, I. Komaromi, R. L. Martin, D. J. Fox, T. Keith, M. A. Al-Laham, C. Y. Peng, A. Nanayakkara, M. Challacombe, P. M. W. Gill, B. Johnson, W. Chen, M. W. Wong, C. Gonzalez, and J. A. Pople, Gaussian03, revision B.05. Gaussian, Inc., Wallingford CT, 2004.